buildings

Article

The Study of the Effects of Supplementary Cementitious Materials (SCMs) on Concrete Compressive Strength at High Temperatures Using Artificial Neural Network Model

Sanaz Ramzi *, Mohammad Javad Moradi and Hamzeh Hajiloo

Department of Civil and Environmental Engineering, Carleton University, Ottawa, ON K1S 5B6, Canada; mjmoradi@cmail.carleton.ca (M.J.M.); hamzehhajiloo@cunet.carleton.ca (H.H.)
* Correspondence: sanazramziaraghi@cmail.carleton.ca

Abstract: In this study, an artificial neural network (ANN) model was developed to predict the compressive strength of concrete containing supplementary cementitious materials (SCMs) at high temperatures. For this purpose, 500 experimental results were collected from the available literature. The effective parameters in the model are the volumes of coarse and fine aggregates, water, cement, coarse-aggregate type, percentage SCMs as the cement replacement, temperature levels, and test methods. The proposed ANN model was developed at a correlation coefficient of 0.966. A parametric study was conducted to evaluate the impact of the combined effects of input parameters (aggregate types and SCM content) on the relative compressive strength of concrete at high temperatures. It was shown that siliceous aggregate has a better performance by producing stronger bonds with cement paste than calcareous aggregates. The optimum SCM contents depend on the aggregate types. The optimum silica fume (SF) content for concrete with a water-to-binder ratio of 0.6 subjected to high temperatures is 8% and 3% for siliceous and calcareous concrete, respectively. The analysis of the ANN model has provided a conclusive understanding of the concrete behaviour at high temperatures.

Keywords: supplementary cementitious materials; high temperatures; artificial neural network; compressive strength

Citation: Ramzi, S.; Moradi, M.J.; Hajiloo, H. The Study of the Effects of Supplementary Cementitious Materials (SCMs) on Concrete Compressive Strength at High Temperatures Using Artificial Neural Network Model. *Buildings* **2023**, *13*, 1337. https://doi.org/10.3390/buildings13051337

Academic Editor: Jan Fořt

Received: 14 April 2023
Revised: 10 May 2023
Accepted: 16 May 2023
Published: 20 May 2023

1. Introduction

A fire can occur during concrete service life, causing severe casualties and property damage [1]. Several mechanical and environmental factors can influence the deterioration of concrete when exposed to high temperatures, such as the level of high temperatures, humidity, the applied load, the heating time, the cooling method after heating, the aggregate type, the mineral admixtures, and the inclusion ratios [2]. Since the aggregates make up 60–75% of the volume of concrete, they significantly affect the behaviour of concrete at room and high temperatures [3]. Coarse aggregates are classified into three groups according to their chemical composition and mineralogical nature: siliceous (Si) aggregate, calcareous (Ca) aggregate, and lightweight aggregate (LWA). Figure 1a shows the chemical compositions (e.g., SiO_2, Al_2O_3, and CaO) of siliceous and calcareous aggregates.

Supplementary cementitious materials (SCMs) such as silica fume (SF), fly ash (FA), and ground-granulated blast furnace slag (GGBFS) are widely used in green concrete as a partial replacement for ordinary Portland cement due to their potential to conserve energy and natural resources and reduce CO_2 emissions [4,5]. The chemical composition of different SCMs, based on their major chemical components (e.g., Al_2O_3, SiO_2 and CaO), are plotted in Figure 1b. Silica fume is a byproduct of the smelting process in silicon and ferrosilicon alloy production. Silica fume mostly consists of silicon dioxide (SiO_2) and extremely fine spherical particles, which lead to its very high pozzolanic activity [6]. Fly ash is a byproduct material generated from coal-firing electricity power plants. Fly ash is composed of silica oxide, iron oxide (Fe_2O_3), aluminium oxide (Al_2O_3), and calcium oxide (CaO) [7]. In fly ash concrete, the pozzolanic reaction of Al_2O_3 and SiO_2 and calcium hydroxide (CaOH) leads to the formation of calcium aluminate hydrate (CAH) and calcium silicate hydrate (CSH), which results in the improvement of strength and durability of concrete [8,9]. The GGBFS, referred to as slag, is also a byproduct of the iron and steel manufacturing process, produced by quenching molten iron slag in steam or water. This granulation process results in the formation of a granulated glassy particle of GGBFS. The main composition of GGBFS particles generally contains calcium oxide, silicon dioxide, magnesium oxide (MgO), and aluminium oxide. GGBFS undergoes hydration reactions due to its hydraulic activity in the presence of water and calcium hydroxide [10,11].

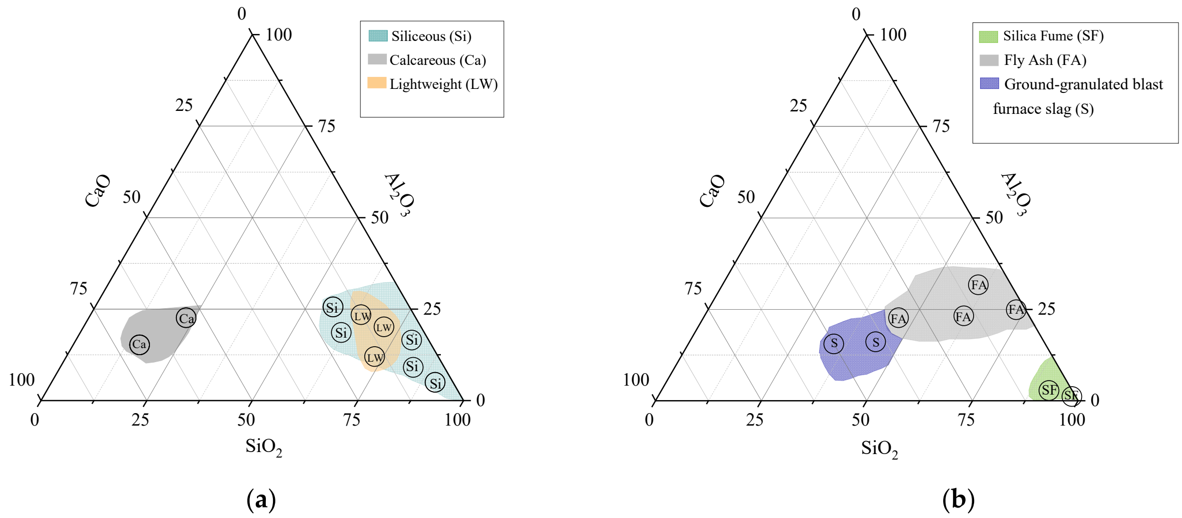

Figure 1. Chemical composition of (**a**) siliceous, calcareous, and lightweight aggregates; (**b**) silica fume, fly ash, and ground-granulated blast furnace slag.

Due to the extensive use of concrete containing SCMs, a comprehensive understanding of how fire impacts the behaviour of concrete is necessary [12]. Many experimental studies investigated the performance of concrete containing different types of admixtures, namely silica fume, fly ash, and ground-granulated blast furnace slag under high-temperature effects. The results revealed that concrete at high temperatures exhibits a nonlinear degradation in mechanical properties. Moreover, there are a number of temperature-dependent parameters and highly complex properties that control concrete response under high-temperature conditions [13]. Therefore, the application of modern evaluating tools, such as the machine-learning (ML) approach, is required to predict the mechanical properties of concrete at high temperatures. The generalization ability and prediction accuracy of machine-learning models are excellent when dealing with nonlinear behaviour [14]. In recent years, the implementation of machine learning, such as artificial neural networks (ANNs), decision trees (DTs), and support-vector machines (SVMs), has acquired considerable attention as an alternative method in solving complex and nonlinear problems [15,16]. Neural networks have been successfully used in different civil engineering problems, such as structural engineering [17], material behaviour modelling [18,19], and detecting structural damage [20].

Several studies have used ML techniques to predict the compressive strength of different concrete types at room temperatures considering various influential parameters. Behnood et al. [21] proposed an ANN-based model to estimate the compressive strength of concrete containing SF at room temperature with acceptable error. It was found that when the percentage of silica fume to binder increased between 0 and 30%, the compressive strength of concrete with silica fume increased linearly. In addition, the maximum aggregate size significantly influences the compressive strength of SF concrete. In another study, Atici et al. [22] developed an ANN and multiple regression analysis (MRA) to estimate the compressive strength of concrete containing different amounts of fly ash and blast furnace slag at various 3, 7, 28, 90, and 180-day curing times. It was concluded that the nonlinear functional relationships in inverse problems, such as designing the concrete mix, could be calculated using the ANN model, which is impossible with classical regression methods. Chopra et al. [23] predicted the compressive strength of concrete with and without fly ash at different curing ages using two computing techniques, genetic programming (GP) and ANN models. It was found that the ANN model using the Levenberg–Marquardt (LM) algorithms for training the network is the most reliable prediction tool for this purpose compared to the GP model. Boğa et al. [24] used an ANN model to predict the mechanical properties and durability properties of concrete that contained ground-granulated blast furnace slag (GGBFS) and calcium nitrite-based corrosion inhibitor (CNI).

There are relatively few studies on the effects of high temperatures on the compressive strength of concrete using the ANN approach. Ahmad et al. [25] evaluated the compressive strength of concrete at high temperatures using different machine-learning techniques, namely ANN and decision tree gradient boosting and bagging. They used 207 data points from the literature, and it was found that the ML algorithms are quite effective in predicting concrete performance at high temperatures. The ANN model showed a better performance compared to the decision tree. However, the bagging model correlation coefficient indicated a better accuracy in comparison to the ANN, decision tree, and gradient boosting. Mukherjee et al. [13] evaluated the behaviour of concrete under three load conditions: a varying load under isothermal conditions (i.e., steady state), a varying temperature under a constant load (i.e., transient temperature state), and a varying temperature under total restraint using ANN models. They used the results of experimental work conducted by Anderberg et al. [26]. Abbas et al. [27] investigated the residual strength of high-strength concrete (HSC) after exposure to high temperatures. Three separate ANN models were developed for siliceous, calcareous, and combined-aggregate concrete. A total of 460 data sets were collected from the literature, of which 177 data points were for calcareous aggregate, 228 data points were for siliceous aggregate, and the rest were either silico-calcareous or unknown aggregate. The variables, including exposure temperature, heating rate, type of coarse aggregate, water-to-binder ratio, aggregate-to-binder ratio, soaking period, and the compressive strength of concrete at room temperature, were selected as inputs for the models. Moreover, according to the sensitivity analysis results, the water-to-binder ratio, elevated temperature, and the compressive strength of concrete at room temperature were the most affecting variables in developing the models for all aggregate types.

The necessity for conducting the current study was identified from the lack of a comprehensive and conclusive understanding of how different concrete mixtures will behave at high temperatures. The literature survey shows few experimental studies on the combined effects of critical factors such as aggregate types, SCM content and temperature level. The use of SCMs in concrete has been proven to be a major milestone towards reducing concrete's carbon footprint. However, its effects on concrete compressive strength at high temperatures should be known to estimate fire safety. Therefore, the present study aims to develop an ANN model to predict the compressive strength of concrete exposed to high temperatures and fully understand the influence of the parameters. For this purpose, a comprehensive database was collected from previous experimental studies considering the most influencing parameters for which sufficient data were available. It is worth mentioning that this study focuses on residual compressive strength as residual test results for concrete containing SCMs more than other tests. Moreover, parametric studies were conducted using the generalization ability of the proposed ANN model to draw conclusive results on the combined effects of key parameters on the residual compressive strength of concrete at high temperatures.

2. Developing Artificial Neural Network (ANN) Models

The artificial neural network predicts the behaviour of the study subject by learning through past experiments and identifying the pattern of the collected data [28]. Generally, a neural network is developed by acquiring and analyzing data and creating a database, determining the architecture, training the network, determining the learning process, and evaluating the generalization of the network after training [29]. The topology of artificial neural networks is similar to the human brain in two aspects: (1) the neural network acquires knowledge from its environment using a learning process and (2) the acquired knowledge is stored in interneuron connections strengths or (synaptic) weights [30]. ANN models are comprised of a large number of neurons, which serve as data processing units. As seen in Figure 2, the general configuration of the neural network is composed of an input layer, one or more hidden layers, and an output layer. The neurons of each layer are connected to all the neurons of the next layers with numerical values known as weights. Weights can be adjusted for every new input data [31]. The input information received by neurons of the input layer is multiplied by the modifiable weights. The sum of the weighted inputs is obtained using the following function (Equation (1)):

$$(net)_j = \sum_{i=1}^{n} \left(x_i \, w_{ij}\right) + b \tag{1}$$

where $(net)_j$ is the weighted sum of the jth neuron for the input received from the preceding layer with n neurons, x_i represents the input value of the input neuron, w_{ij} is the weight between i neuron of the input layer and j neuron in the next layer, and b is a fixed value called bias. The summation results are then transmitted to neurons in the hidden layer. Each hidden neuron processes information through an activation function and sends its output to the neurons of the output layer. This data is multiplied by the corresponding weights between the hidden layer and output layer, and then their sum is calculated and transmitted to the output layer [24,32]. Then, another activation function is applied to this data, and the output of the network is computed in the output layer. The ANN model outputs are then compared to the desired outputs (experimental results) to determine the error of the network. In order to minimize training errors, the output layer passes the error back to the input layer, and the network's weights and biases are adjusted using an error back-propagation algorithm. This training cycle, known as an epoch, is continued until the error is decreased to an acceptable level [33,34]. Various algorithms have been used for training ANN models, including the back-propagation algorithm, the simulating annealing algorithm, the genetic algorithm, and the particle-swarm optimization algorithm [35]. The back-propagation algorithm is one of the most common training algorithms, using the gradient-descent approach that modifies the weights for a particular training pattern to minimize error [29].

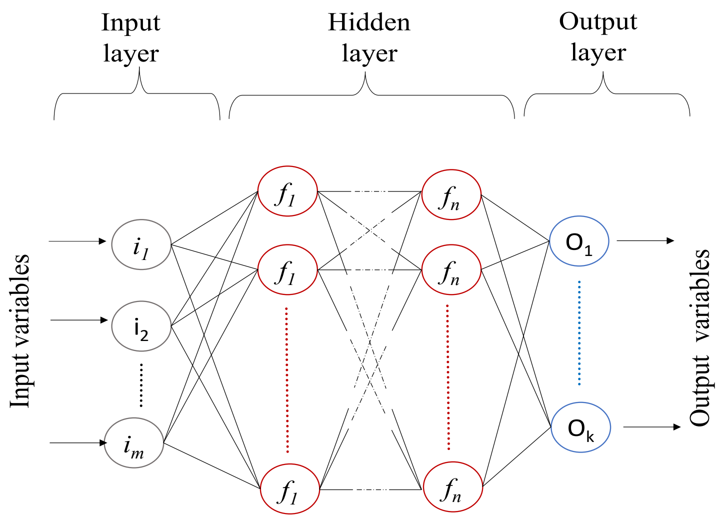

Figure 2. Typical architecture of the artificial neural network with hidden layer.

2.1. Database

A sufficiently large database is required to cover the range of affective variables and their combinations to use the ANN [27]. Generally, an indepth literature review or a comprehensive testing program is required to identify the influential parameters and develop the database. In order to accelerate the learning process and achieve faster convergence as well as generate values in the 0–1 range by the activation functions, the content of the database before the training process must be normalized within the 0–1 range using linear Equation (2) [18,36]:

$$x_{normalized} = \frac{x - x_{min}}{x_{max} - x_{min}} \tag{2}$$

where $x_{normalized}$, x_{min}, and x_{max} denote the normalized, minimum, and maximum values of x as input or output variables, respectively.

An optimized ANN model for predicting the compressive strength of concrete exposed to high temperatures was developed by collecting a comprehensive database containing 500 experimental data from the published literature [6,37–47]. Table A1 represents the collected data from the literature review. The parameters, namely temperature level, type of coarse aggregate, percentage of SCMs (SF, FA, and GGBFS) as the cement replacement, the amount of cement, coarse and fine aggregate, water content, and test methods, namely transient (TR), steady-state (SS), and residual (R), were selected as input variables. The relative compressive strength, defined as the ratio of the compressive strength of concrete at a given temperature to the initial compressive strength of concrete at room temperature, was considered the output of the ANN-based model.

It should be noted that the variation in the heating rate in the collected experimental records was between 0.77 °C/min and 25 °C/min. The heating rate affects the spalling behaviour of concrete, and a fast heating rate increases the temperature differences between the surface and inner parts of concrete resulting in elevated tensile stresses [48]. In addition, the heating rate could not influence the residual compressive strength [49]. The database in this study contains only the specimens that did not spall during or after a high-temperature exposure. In addition, many experimental studies did not accurately report the heating rates. Therefore, in this study, the heating rate was not included in the input parameters of the ANN. The statistical properties of collected data sets are represented in Table 1. The distribution of each quantitative input parameter in the data set is shown in Figure 3. In addition, the frequency of different SCMs (SF, FA, and GGBFS) and the various test methods for three types of aggregate, namely, siliceous, calcareous, and lightweight aggregate, are shown in Figure 4. Out of the total 500 data points, there were 306 data points for the residual test, 114 data points for the transient test, and 80 data points for the steady-state test method. The studies on lightweight aggregate are considerably limited compared to other types of aggregate, as seen in Figure 4, and for this reason, the effects of lightweight aggregate were only considered in Section 3.1, where the effects of test methods were evaluated using the ANN model.

Table 1. Statistics of the quantitative input parameters used in the ANN model.

Attribute	Unit	Max	Min	Average	Standard Deviation
Temperature	°C	870	95	391.5	224.8
Coarse aggregate	kg/m^3	1200	369	950	187.1
Fine aggregate	kg/m^3	880	536	732.2	90.1
Cement	kg/m^3	662	180	406	131.1
Water	kg/m^3	250	127	174.8	28
Silica fume	%	10	5	8.91	1.76
Fly ash	%	60	10	25	14.02
ground-granulated blast furnace slag	%	40	30	35	5.16
Relative compressive strength		1.37	0.07	0.7	0.026

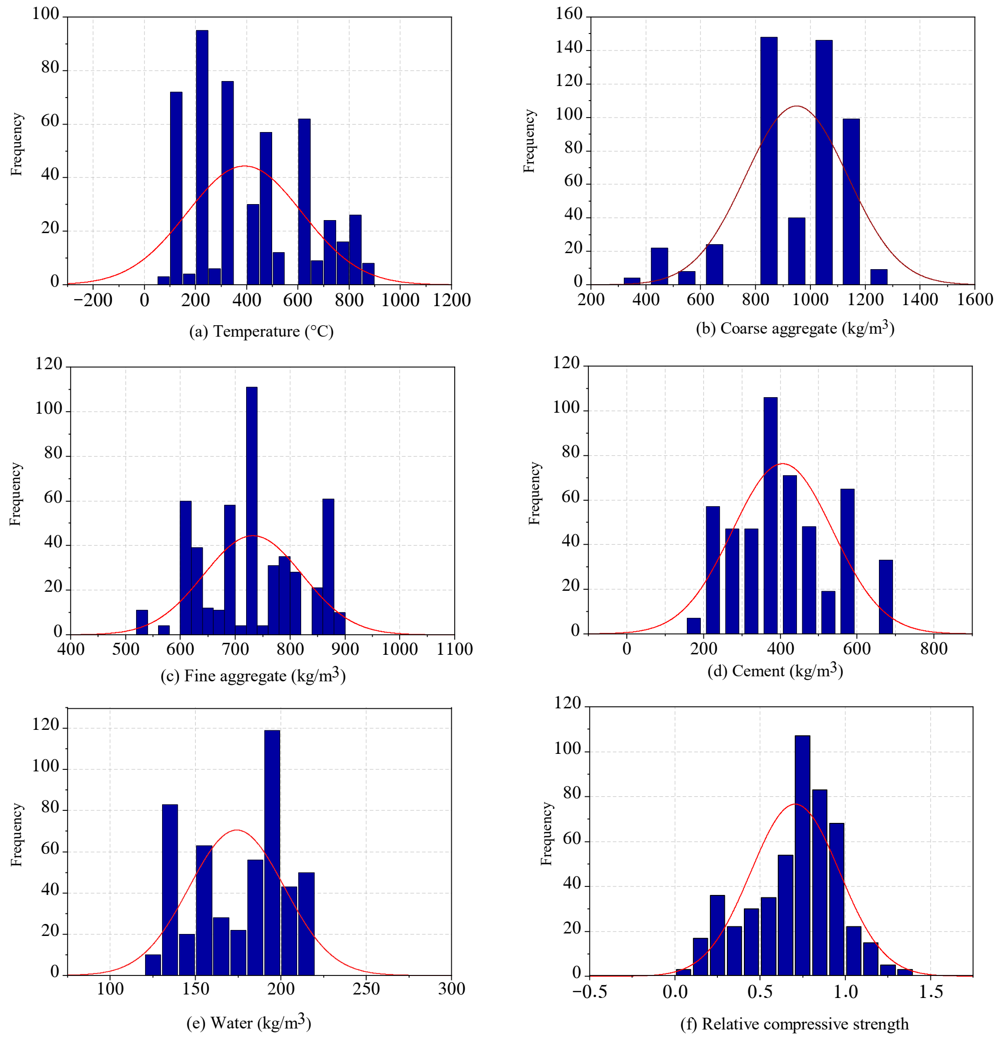

Figure 3. The histograms of the frequency distribution of input and target parameters. Red lines over the data histogram represent the normal distribution curve.

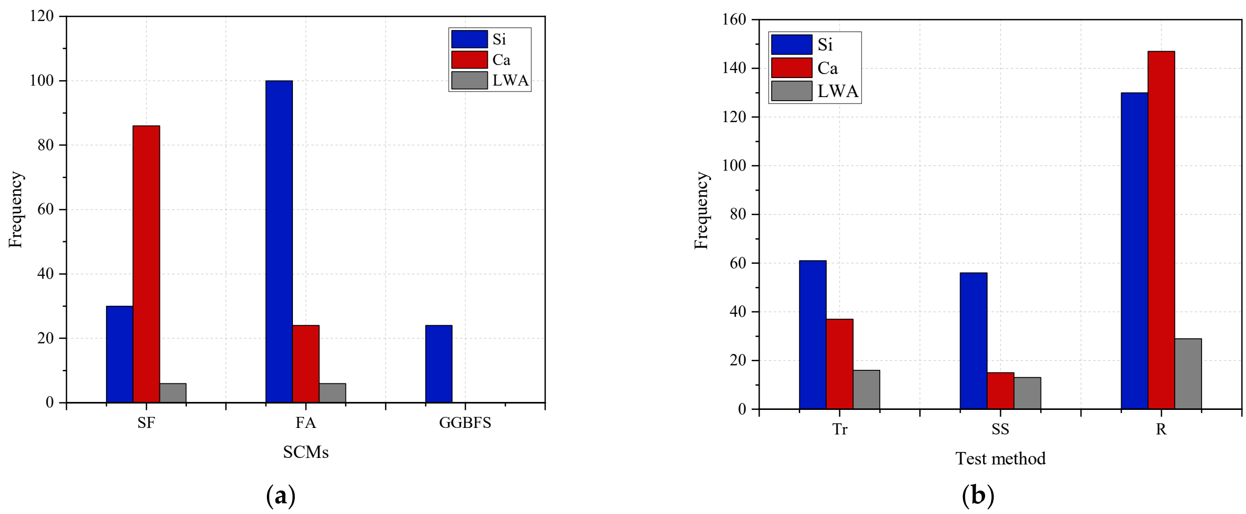

Figure 4. Distribution of (**a**) different types of SCMs (SF, FA, and GGBFS) and (**b**) test methods (Tr, SS, and R) in the database.

2.2. Limitations, Assumptions, and the Orientations of This Study

The criteria used in the development of the database are summarized below:

1. The database only contains air-cooled concrete after the heating period for the residual test method.
2. The data covers concrete specimens containing no fibres.
3. The heating rate was not included in the input parameters.

In this study, the data from three test methods, including stressed, unstressed, and residual, were collected to develop the ANN model. The procedure and the assumptions in developing the ANN model in this study are described in Section 2.2. After developing the model, the effects of varying input parameters on the compressive strength of concrete were investigated using the predictions of the model. Since the residual test results are more than other test methods for concrete-containing SCMs, this research focuses on the residual compressive strength, as discussed in Section 3. In addition, two significant parameters, test methods and water-to-cement (w/c) ratios which affect the compressive strength of concrete subjected to high temperatures, were discussed in Sections 3.1 and 3.2, respectively.

2.3. Modeling the Network

After creating the database, the critical step is identifying the best architecture of the model. Generally, the ANN model consists of the input, hidden, and output layers. Input and output parameters determine the number of neurons in input and output layers. Therefore, to achieve the best architecture of an artificial neural network, the number of hidden layers and their neurons should be chosen appropriately. There is no general method for selecting the number of neurons in the hidden layer to establish an ANN model for a particular problem. The number of neurons in the hidden layer is determined through the trial-and-error method. Thus, the number of neurons in the hidden layers can be started with a small number, increasing progressively while monitoring the error of the network. Finally, the optimum number of hidden neurons is obtained based on the error criteria or performance of the network [19,50]. In the present study, a source code was used in the MATLAB program to operate the trial-and-error process automatically.

Activation functions are selected based on the types of data and layers available. The neurons calculate their output using an activation function based on the weighted inputs that they receive. There are three different types of activation functions commonly used in artificial neural networks, namely the hyperbolic tangent sigmoid (TANSIG), logarithmic sigmoid (LOGSIG), and linear transfer (PURLIN) function. This study employed Tansig and Purlin activation functions in the hidden layer and output layer, as represented in Equations (3) and (4), respectively [51].

$$y = TANSIG = \frac{2}{1 + e^{-2x}} - 1 \tag{3}$$

$$y = PURLIN = x \tag{4}$$

There are different training algorithms in the MATLAB environment, such as scaled conjugate gradient back, Levenberg–Marquardt (LM), Bayesian Regularization, etc. Due to the high precision and suitable and fast convergence, the Levenberg–Marquardt algorithm was used to train the network [28].

The best configuration of the network is reached by trial and error. Different architectures containing one hidden layer with varying numbers of neurons in the hidden layer have been tested to achieve the best structure of the proposed model using the MATLAB program, and simultaneously the error values for each number of neurons in the hidden layer were checked. Finally, a model with a suitable error consisting of twelve neurons in one hidden layer was selected to estimate the relative compressive strength of concrete at high temperatures, as depicted in Figure 5.

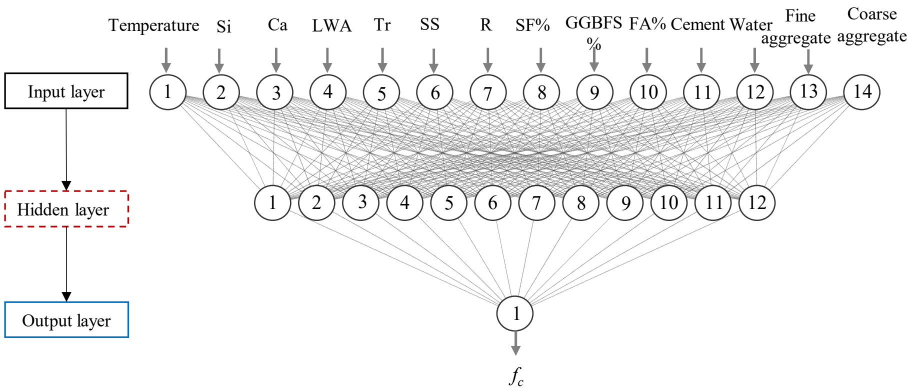

Figure 5. The architecture of the proposed ANN model. The circles indicate the number of neurons in each layer.

2.4. Performance of the ANN Models

Generally, the ANN models are developed using three main datasets: training, validation, and testing. Therefore, the database was randomly divided into three subsets in order to achieve a good generalization: training, validation, and testing sets. The training data is used for training the model by adjusting modifiable weights between layers. As part of the training process, the validation data sets are used to evaluate the model's fit on training data and refrain from overfitting by stopping the training. The testing data set is used to measure the generalization capability of the model [52]. In the present study, by default in MATLAB, the database is randomly divided into three subsets: 70% of total data points for training, 15% for validation, and 15% for testing.

In this study, statistical error estimation methods, including mean square error (MSE), root mean square error (RMSE) and correlation coefficient (R), are employed to assess the adequacy and precision of the networks according to the following equations:

$$MSE = \frac{1}{N} \sum_{i=1}^{N} (y_i - \hat{y}_i)^2 \tag{5}$$

$$RMSE = \sqrt{\frac{1}{N} \sum_{i=1}^{N} (y_i - \hat{y}_i)^2} \tag{6}$$

$$R = \frac{\sum (\hat{y} - \overline{\hat{y}})(y - \overline{y})}{\sqrt{\sum (\hat{y} - \overline{\hat{y}})^2} \sqrt{\sum (y - \overline{y})^2}} \tag{7}$$

where $\overline{y}$ and $\overline{\hat{y}}$ demonstrate the average values of the target and predicted outputs; y and $\hat{y}$ are the target and predicted values of the network, respectively. The values obtained for MSE, RMSE, and R are listed in Table 2. Moreover, in order to assess the performance of data, plots of the mean square error versus epoch (number of iterations) are used for training, validation, and testing [53]. Figure 6 shows the performance of the networks in predicting the compressive strength established in the MATLAB program. The blue line represents the decreasing mean square error of the training data set. The green line shows the validation error, which monitors the overfitting of the network [54]. Overfitting occurs in the network when the validation-error data begins rising [55]. The red line indicates the error of the test data used to determine the generalization capability of the model. The best performance is achieved at the lowest validation error when there is no further increase in MSE error [53–55]. The best validation of the performance of the proposed compressive strength ANN model was obtained at epoch 18, with a mean square error (MSE) of 0.00477, as shown in Figure 6.

Table 2. Performance measurements of the proposed ANN model.

Dataset	Performance Metric		
	R	**MSE**	**RMSE**
Training	0.98	0.0019	0.0436
Validation	0.94	0.0048	0.0693
Testing	0.95	0.0042	0.0648
All data	0.97	0.0027	0.0164

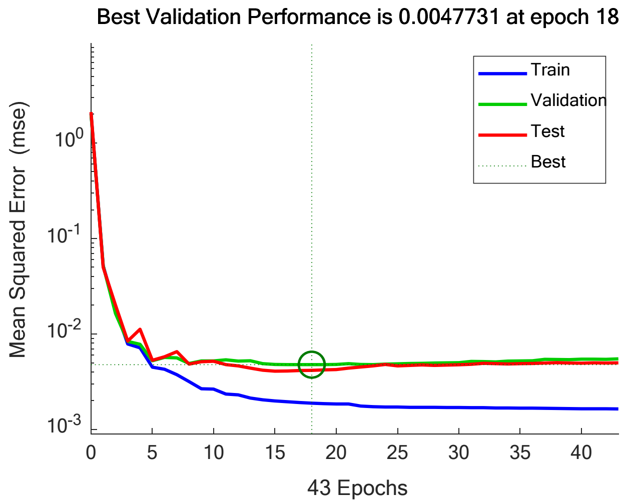

Figure 6. The performance of the proposed ANN model. The green circle represents the best validation performance.

The coefficient of correlation (R), indicating the correlation between the target and predicted (output) values for train, validation, and testing, and all data points, is shown in Figure 7a–d. It can be seen that the coefficient of correlation for all data points was 0.966 for the developed ANN model. The optimal value for R is one, and the optimal value for MSE and RMSE is zero [56]. Thus, the obtained values-of-error metrics indicate the satisfactory performance of the proposed network with a large number of input variables. The comparison of prediction results of the ANN model and the experimental data points of the relative compressive strength of concrete is illustrated in Figure 8. It can be seen that the ANN model predicts the experimental results with acceptable accuracy.

2.5. Sensitivity Analysis

The sensitivity analysis is used to determine how input variables contribute to the output of a network. In this way, the user can reduce the size of the network by eliminating insignificant input parameters [57]. This technique identifies the most important input parameters considered by the network. The results of the sensitivity analysis in this study are shown in Figure 9. It revealed that the temperature level is the most important parameter in the results of the developed ANN-based models compared to other input variables.

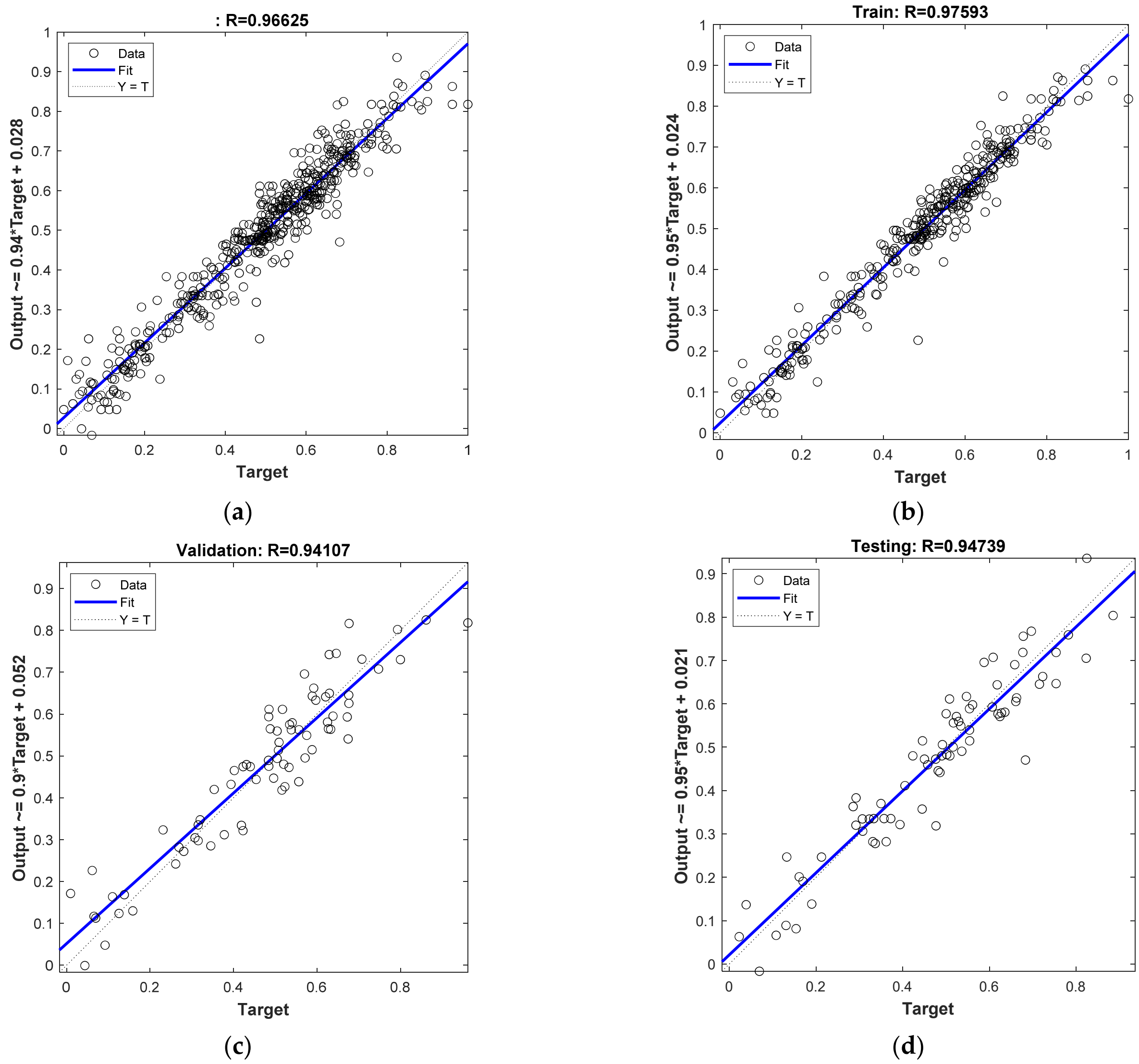

Figure 7. The regression plots of the proposed ANN model for (**a**) all data, (**b**) training, (**c**) validation, and (**d**) testing.

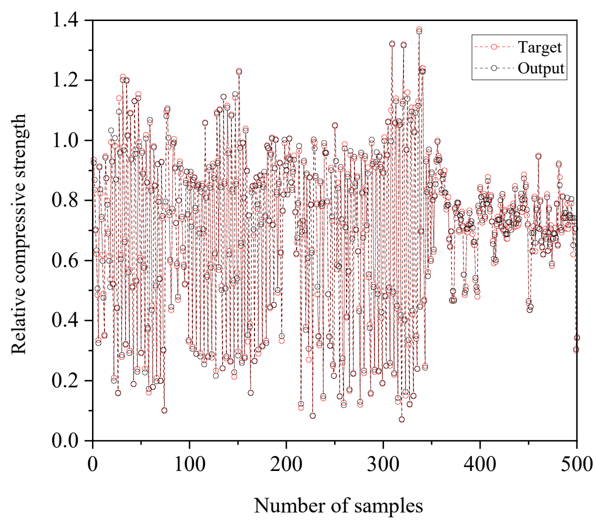

Figure 8. The comparison of experimental data (target) and the predicted results (output) of the developed ANN model.

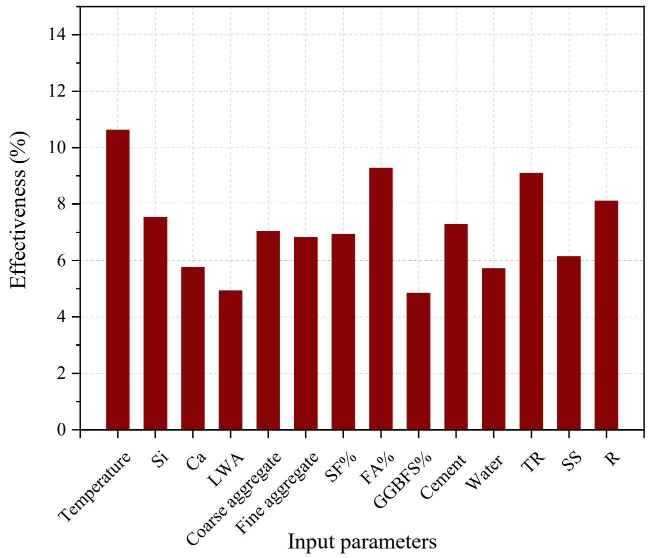

Figure 9. Sensitivity analysis of the selected model for the compressive strength of concrete at high temperatures.

3. Parametric Studies

An ANN-based model was developed to predict the mechanical characteristics of concrete exposed to high temperatures, and its performance was evaluated. Due to the generalization capability of the neural network, the influence of the input variables on the output can be examined using a parametric study [58]. Patterns similar, but not identical, to those with which ANN models have been trained can be recognized and answered by the models in a parametric study [59]. In the following sections, parametric analysis was carried out to evaluate the effect of input variables on the strength of concrete using the prediction of the suggested ANN model. In the parametric study, the values of input parameters, except those being examined, were constant.

3.1. The Effects of Three High-Temperature Test Methods on Compressive Strength

Typically, three test methods are used to determine the properties of concrete exposed to high temperatures, including transient, steady-state, and residual tests. In the transient test, the specimens are first loaded (20–40% of ultimate compressive strength), and this loading is sustained during heating until the failure of the specimens. In the steady-state test, the concrete specimens are heated (without a preload). Once the specimens reach a uniform temperature, they are loaded to failure. The concrete specimens in the residual test method are heated to the target temperature without a preload until specimens reach a thermal steady state. After the specimens are cooled to room temperature, the load is applied until failure occurs [3,60,61]. In this study, the term 'residual compressive strength' refers to the compressive strength of the concrete obtained based on residual test methods data. The outcomes of the ANN model for three test methods (transient, steady-state, and residual) for concrete with a water-to-cement ratio of 0.5 are compared to ACI 216.1 [62] and Eurocode [63] results for siliceous, calcareous, and lightweight concrete in Figure 10a–c, respectively. It should be mentioned that the Eurocode model is limited to the transient tests, and it does not cover the relative compressive strength of lightweight concrete. Table 3 lists all the assumed concrete-mix designs for three different aggregate types selected for a parametric study on compressive strength. The range of temperature was selected between 20 °C and 800 °C.

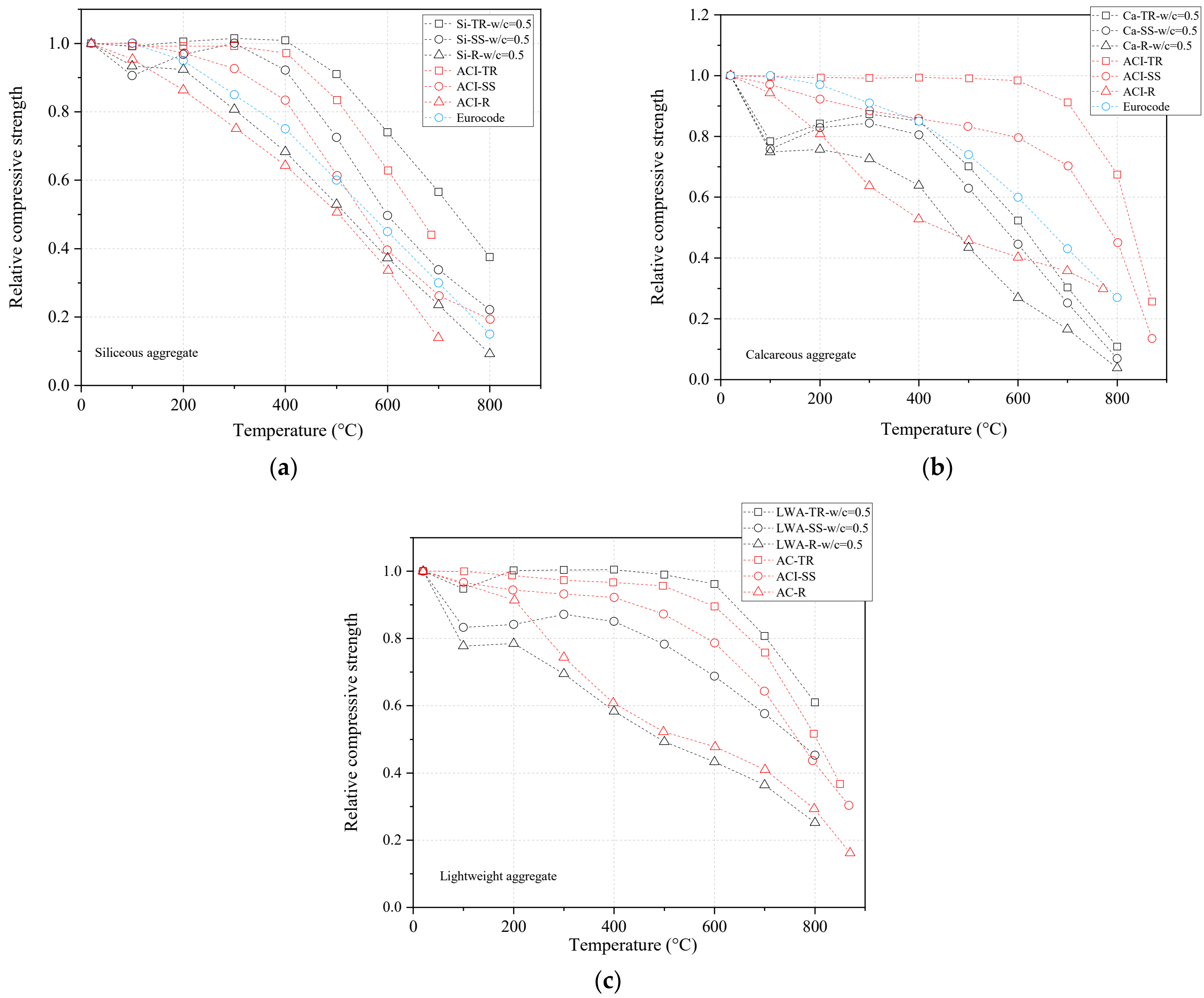

Figure 10. The comparison of the results of the proposed ANN model for (**a**) siliceous concrete, (**b**) calcareous concrete, and (**c**) lightweight concrete under three test methods (TR, SS, and R) exposed to high temperatures with ACI 216.1 [62] and Eurocode [63] results.

Table 3. The concrete-mix designs for parametric analysis of the effects of the high-temperature test methods on the relative compressive strength [40,41,43,46].

Number	Coarse-Aggregate Type	Coarse Aggregate (kg/m^3)	Fine Aggregate (kg/m^3)	SF%	FA%	GGBFS%	Cement (kg/m^3)	Water (kg/m^3)	w/c	Used in
1	Si	1080	855	0	0	0	249	127	0.50	Test method
2	Ca	1095	795	0	0	0	320	160	0.50	
3	LWA	482	678	0	0	0	370	185	0.50	

Overall, the lowest relative compressive-strength loss was observed in the transient test, followed by the steady-state and residual tests for all types of aggregate. Although it is difficult to generalize the effects of the three different test methods on concrete remaining strength at high temperatures, the better strength in transient tests could be attributed to the friction caused by the preloading of specimens, limiting the thermal stress in the expansion of the specimens, thereby preventing thermal cracking caused by the thermal gradient. Moreover, preloading can densify the concrete pore structure by compressing the coarsened pores caused by high temperatures [64,65]. The effects of sustained load during transient tests can cause premature spalling, especially for load ratios of 70% [66].

It can be seen in Figure 10a that the results predicted by the proposed ANN model for siliceous concrete are relatively close to the results of ACI 216.1 [62]. In the case of calcareous-aggregate concrete, there is a considerable difference between the results of ACI 216.1 and the prediction of the ANN model, as shown in Figure 10b. However, the results of Eurocode [63] were close to the ANN results. The outcomes of the ANN model compared to the ACI 216.1 result for lightweight concrete are plotted in Figure 10c. It was found that the prediction of the model for the relative compressive strength of lightweight concrete was in close agreement with the ACI216.1 results of all test methods.

3.2. The Effects of Water-to-Cement Ratio on Residual Compressive Strength

The relative compressive strength at three different water-to-cement ratios of 0.3, 0.5, and 0.6 for siliceous and calcareous concrete subjected to high temperatures up to 800 °C compared to the results of the ACI 216.1 [62] and Eurocode [63] are shown in Figures 11 and 12, respectively. The assumed concrete-mix designs for investigating the influence of w/c ratios are shown in Table 4. The results of the ANN model were only presented for the residual test due to a wide range of data in this test approach (see Figure 4b). According to Eurocode, high-strength concrete is classified into three classes based on its compressive strength: C 55/67 and C 60/75 is Class 1, C 70/85 and C80/95 is Class 2, and C90/105 is Class 3. The compressive strength of analyzed data in the ANN model fell within the category of Class 2 in Eurocode. As seen in Figure 11, at 100 °C, the relative compressive strength of siliceous aggregate concrete was reduced due to free water from concrete evaporation. Between 100 °C and 300 °C, the strength improved or remained constant. Beyond 300 °C, the compressive strength was reduced with temperature rise. Compressive strength improved due to the increasing forces between the particles of CSH particles by removing interlayer water [67]. Regarding calcareous-aggregate concrete with a w/c of 0.3, the compressive strength reduced continuously with increasing temperature. However, in the case of higher w/c (0.5 and 0.6), significant strength loss occurred up to 100 °C by evaporation of water. A compressive-strength recovery was observed after heating to 200 °C compared to 100 °C. Above 300 °C, for calcareous concrete severe compressive-strength loss occurred due to the decomposition of CSH and the generation of inner cracks. The formation of cracks could be attributed to the inner thermal stresses caused by the thermal expansion of aggregates and cement paste shrinkage [37]. Overall, higher w/c ratios for both siliceous and calcareous aggregate result in more strength loss after heat exposure. This can be explained by the increasing pore diameter and coarsening of the pore structure [38,68]. Eurocode [63] provides predictions only in hot conditions, indicating that the reduction of compressive strength was lower in normal-strength concrete compared to HSC. ACI 216.1 [62] and Eurocode results are conservative compared to the ANN-based model predictions, as shown in Figures 11 and 12.

Table 4. The concrete-mix designs for parametric analysis of the effect of water-to-cement ratios on the residual compressive strength.

Number	Coarse-Aggregate Type	Coarse Aggregate (kg/m^3)	Fine Aggregate (kg/m^3)	SF%	FA%	GGBFS%	Cement (kg/m^3)	Water (kg/m^3)	w/c	Used in
1	Si	1086	724	0	0	0	500	150	0.3	
2	Si	1132	609	0	0	0	410	205	0.5	
3	Si	1050	699	0	0	0	343	205	0.6	Effect of w/c
4	Ca	1168	615	0	0	0	495	149	0.3	
5	Ca	854	868	0	0	0	392	196	0.5	
6	Ca	854	868	0	0	0	368	221	0.6	

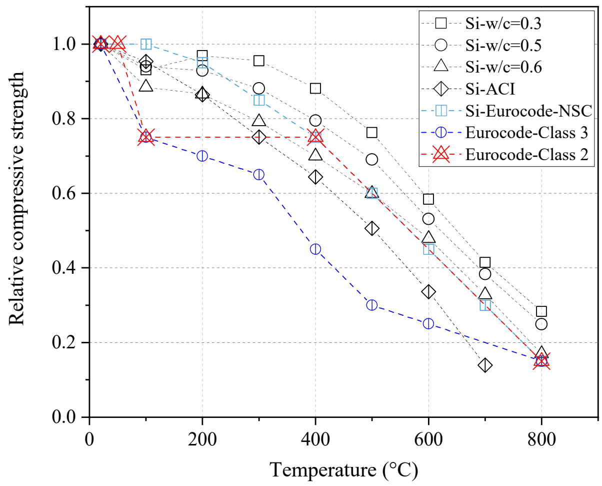

Figure 11. Comparison of prediction of the proposed ANN model for siliceous concrete with three w/c: 0.3, 0.5, and 0.6 exposed to high temperatures with Eurocode [63] and ACI 216.1 [62] results.

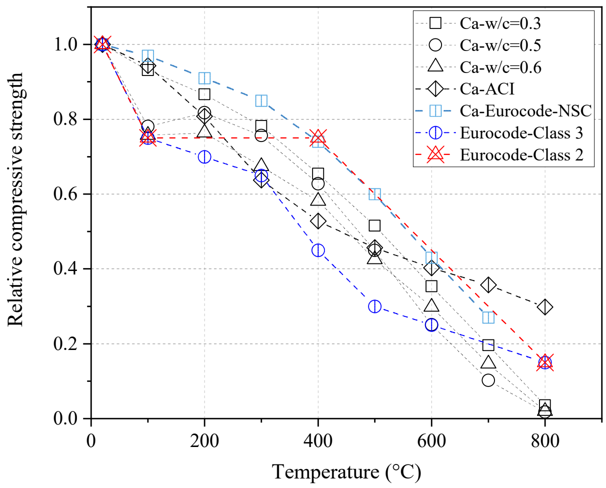

Figure 12. Comparison of prediction of the proposed ANN model for calcareous concrete with three w/c: 0.3, 0.5, and 0.6 exposed to high temperatures with Eurocode [63] and ACI 216.1 [62] results.

3.3. The Effects of Supplementary Cementitious Materials on Residual Compressive Strength

In order to analyze the effect of the replacement of cement with different SCMs, the relative compressive strength of concrete containing different contents of silica fume (0%, 5%, and 10%), fly ash (0%, 20%, 30%, and 40%), and ground-granulated blast furnace slag (0%, 30%, and 40%) at high temperatures up to 800 °C was investigated. The selected mix designs are represented in Table 5. It is worth noting that the provisions of both ACI 216.1 [62] and Eurocode [63] have not covered the effect of SCMs on the compressive strength of concrete at high temperatures.

3.3.1. The Effects of Silica Fume (SF)

The available research works are limited to high-strength concrete containing SF at 0–10% cement-replacement ratios. Accordingly, this study examines incorporating SF at replacement levels of 0%, 5%, and 10 % on the compressive strength of concrete with a water-to-binder ratio of 0.3. The prediction of the network for siliceous concrete compared to calcareous concrete exposed to high temperatures up to 800 °C is depicted in Figure 13. It can be seen that the concrete without SF shows slightly better performance than the SF concrete, particularly for 10% SF replacement for both Ca and Si aggregate concrete. Concrete containing SF exhibits a denser interfacial transition zone (ITZ) between cement paste and aggregates due to the filler effect of ultrafine particles and the pozzolanic activity of SF compared to ordinary Portland cement (OPC) concrete. Therefore, higher stress levels are produced in the ITZ because of the expansion of aggregate and contraction of paste with SF than that of the OPC concrete exposed to high temperatures. This causes more reduction in the relative compressive strength of SF concrete [6,64].

Table 5. The concrete-mix designs were employed for parametric analysis of the effect of different SCMs on the relative compressive strength of concrete [6,38–40,43].

Number	Coarse-Aggregate Type	Coarse Aggregate (kg/m^3)	Fine Aggregate (kg/m^3)	SF%	FA%	GGBFS%	Cement (kg/m^3)	Water (kg/m^3)	w/b	Used in
1	Ca	1168	615	0	0	0	495	149	0.30	Effects of SF
2	Ca	1168	615	5	0	0	470	149	0.30	
3	Ca	1168	615	10	0	0	445.5	149	0.30	
4	Si	1066	710	0	0	0	500	150	0.30	
5	Si	1066	710	5	0	0	475	150	0.30	
6	Si	1066	710	10	0	0	450	150	0.30	
7	Si	1196	643	0	0	0	450	135	0.30	Effects of FA
8	Si	1196	643	0	20	0	360	135	0.30	
9	Si	1196	643	0	30	0	315	135	0.30	
10	Si	1196	643	0	40	0	270	135	0.30	
11	Si	1095	795	0	0	0	300	180	0.60	
12	Si	1095	795	0	20	0	240	180	0.60	
13	Si	1095	795	0	30	0	210	180	0.60	
14	Si	1095	795	0	40	0	180	180	0.60	
15	Ca	846	734	0	0	0	662	199	0.60	
16	Ca	846	734	0	20	0	530	199	0.60	
17	Ca	846	734	0	30	0	463	199	0.60	
18	Ca	846	734	0	40	0	397	199	0.60	
19	Si	1145	616	0	0	0	500	150	0.30	Effect of GGBFS
20	Si	1145	616	0	0	30	350	150	0.30	
21	Si	1145	616	0	0	40	300	150	0.30	
22	Si	1135	626	0	0	0	390	195	0.50	
23	Si	1135	626	0	0	30	273	195	0.50	
24	Si	1135	626	0	0	40	234	195	0.50	

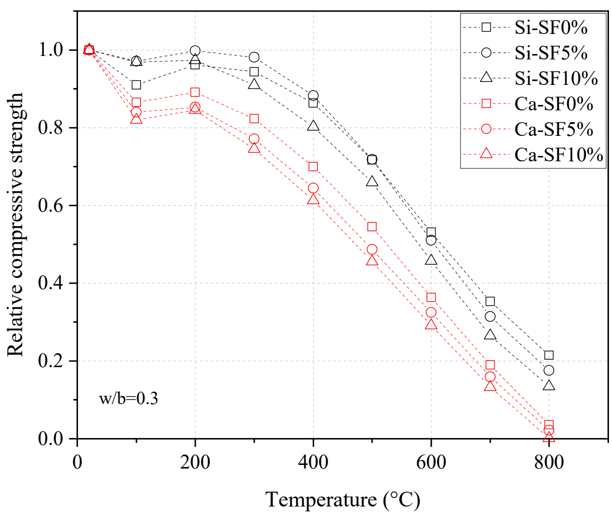

Figure 13. The influence of SF content on the relative compressive strength of siliceous or calcareous concrete with w/b of 0.3 exposed to high temperature using the proposed ANN model.

3.3.2. The Effects of Fly Ash (FA)

The influence of different contents of FA (0%, 20%, 30%, and 40%) on the compressive strength of siliceous aggregate concrete at w/b of 0.3 and 0.6 are plotted in Figure 14. The inclusion of FA increases the relative compressive strength of concrete compared to concrete without FA at all temperatures. However, the presence of FA in improving the relative compressive strength of siliceous concrete is notable up to 400 °C. Beyond this temperature, there is nearly no difference between 20%, 30%, and 40% FA concrete. The better performance of FA concrete is due to the pozzolanic reaction of FA particles and calcium hydroxide and the production of C–S–H gel which increases the strength of the concrete [46]. The addition of FA is slightly more effective in siliceous concrete with lower w/b.

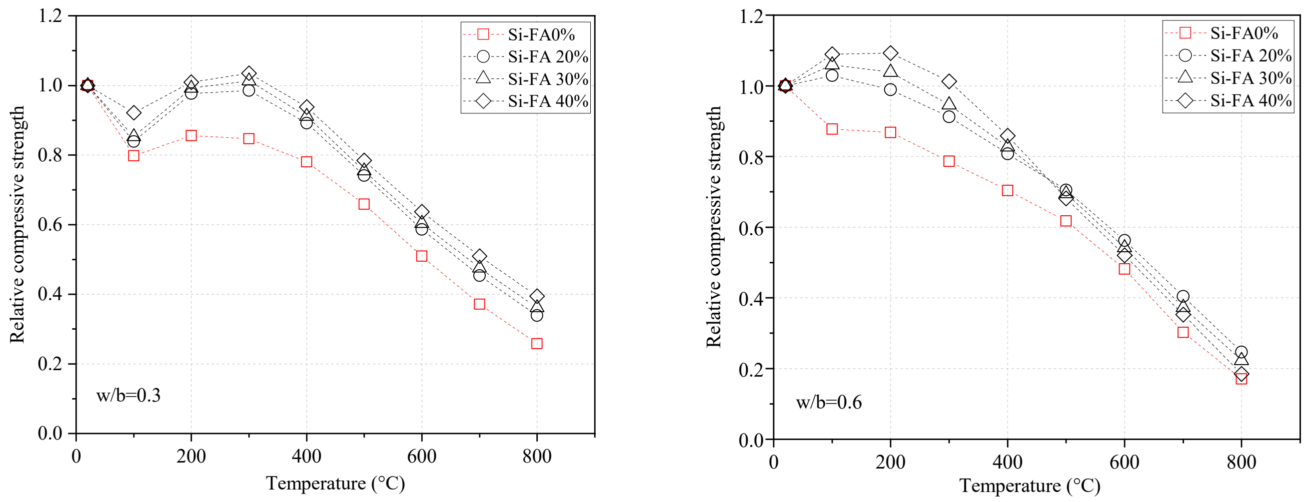

Figure 14. The influence of FA content on the relative compressive strength of siliceous (**a**) with w/b of 0.3 and (**b**) with w/b of 0.6 exposed to high temperature using the proposed ANN model.

The results were investigated only for calcareous concrete with a w/b ratio of 0.6 because there is insufficient data available in the literature for calcareous concrete with lower w/b ratios. Overall, Figure 15 shows a lower improvement in the compressive strength at high temperatures of calcareous concrete compared to siliceous concrete. Once compared with 0% FA concrete, the relative compressive strength tends to decrease with increasing the FA content up to 40%. The better performance of FA concrete compared to concrete without FA can be attributed to the pozzolanic reaction of reactive SiO_2 from FA and $Ca(OH)_2$ from cement, resulting in the reduction of the $Ca(OH)_2$ amount in the concrete [69]. The presence of FA keeps the relative strength of concrete near and over 1.0 up to 300 °C. However, the compressive strength reduced with temperature rise. Similar results were reported in experimental research carried out by Savva et al. [43]. Overall, the relative compressive strength was over 15% and 10% higher for silicious and calcareous FA-contained concrete up to 400 °C, respectively, compared to OPC concrete.

3.3.3. The Effects of Ground-Granulated Blast Furnace Slag (GGBFS)

The results of the ANN model for three siliceous concrete mixes with different levels of GGBFS (0%, 30% and 40%) and two w/b ratios (0.3 and 0.5) are depicted in Figure 16. Before 300 °C and 200 °C, there is no significant reduction except at 100 °C for concrete with w/b ratios of 0.3 and 0.5, respectively. Beyond 300 °C, the compressive strength decreased linearly for all concrete mixes. For concrete with w/b of 0.3, the cement replacement with GGBFS led to slightly better performance than concrete without GGBFS. This can be explained by the acceleration of the hydration reaction caused by the increase in temperature [38,70]. It should be noted because the data for calcareous concrete containing GGBFS is not available in the literature (see Figure 4a), the results of the model were generated only for Si concrete containing GGBFS in the parametric study.

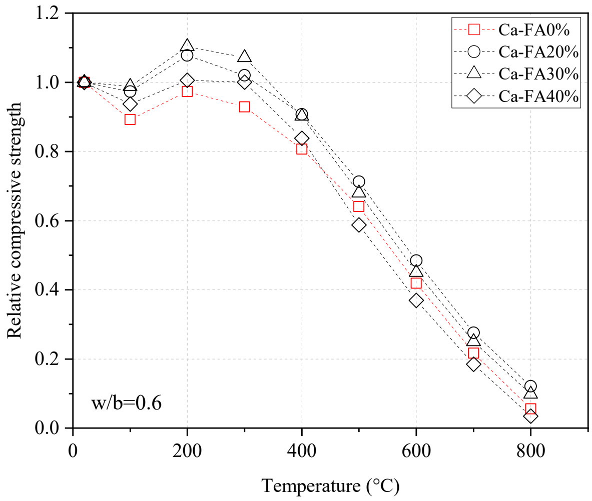

Figure 15. The influence of FA content on relative compressive strength of calcareous concrete with w/b of 0.6 exposed to high temperature using the proposed ANN model.

3.3.4. Combined Effects of Aggregate Types and SCMs

Studying the combined effects of parameters on concrete strength subjected to high temperatures is beneficial. The lack of comprehensive experimental studies that have considered nearly all of the key parameters highlights the ANN contribution to combine the results of multiple studies and generate a holistic understating of the concurrent effects of varying parameters. To the authors' knowledge, no experimental studies have investigated the effects of aggregate types on SCM concrete. Figure 17 shows the predictions of the ANN model for the residual compressive strength of concrete-containing SCMs along with the two aggregate classes (i.e., siliceous and calcareous) at temperatures up to 800 °C. To understand the combined effect of SCMs class and aggregate type, the chemical composition of binder and aggregate needs to be considered. Several studies investigated the chemical reaction between binder and aggregate [71–76]. It was shown that siliceous aggregate produces a stronger bond with cement paste by providing a chemical reaction between quartz (abundant in siliceous aggregate) and $Ca(OH)_2$ as well as a higher C-S-H formation rate in concrete with siliceous aggregates [77,78]. As Figure 17 indicates, the Figure 17 compressive strength of concrete made by siliceous aggregate is higher; this agrees with the results of the study reported by Savva et al. [43], in which the effect of high temperatures on the compressive strength of concrete containing FA with different aggregates was investigated. The results of the ANN model demonstrated in Figure 17 prove the multifactored effect of high temperatures along with the presence of interaction between different aggregate types and SCMs. The multifactored effect of various parameters may explain the contradictory results of studies on the compressive strength of concrete subjected to high temperatures [79–82].

Around 100–300 °C, the compressive strength of various mixtures slightly increases or remains unchanged. This may be attributed to the possibility of steam curing resulting in additional hydration of unhydrated cement particles at temperatures 100–300 °C [43,83]. Additional hydration can be revealed by a decrease in phases (C_3S + β-C_2S) and an increase in the content of $Ca(OH)_2$ [84]. Moreover, by comparing the results, it can be concluded that the temperature in which the maximum compressive strength occurs is almost the same for each SCM, and it is independent of aggregate type. This may be due to the dehydration of C-S-H, ettringite, and calcium aluminate hydrates which mainly depends on the ratio of CaO/SiO_2 of the binder [85–87].

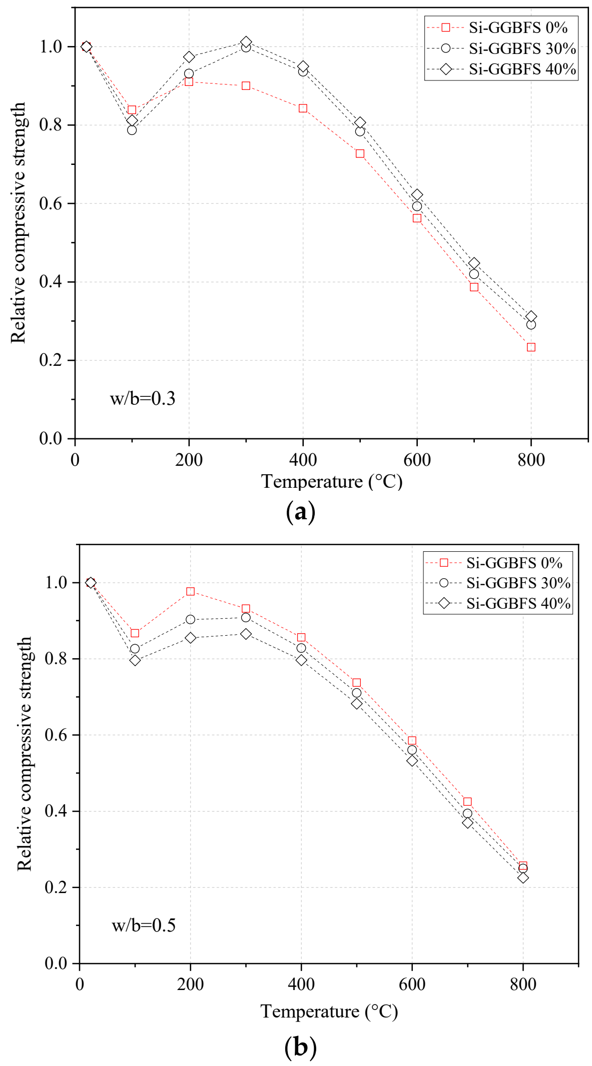

Figure 16. The influence of GGBFS content on the relative compressive strength of siliceous concrete (**a**) with w/b = 0.3 and (**b**) with w/b = 0.5 exposed to high temperature using the proposed ANN model.

On the other hand, aggregates with different chemical compositions have a distinctive thermal response. The thermal degradation for siliceous aggregates, inducing internal stresses, occurs at around 570 °C. The main reason can be attributed to the chemical composition in which the quartz crystal softens and the α–β of quartz transforms to an intermediate incommensurate phase [88,89]. The main reason for a defect in calcareous aggregate is the decarbonation of calcium carbonate ($CaCO_3$), producing more calcium oxide (CaO). The subsequent hydration of the new CaO increases the aggregate volume (almost 40% anisotropic expansion) and subsequently weakens the structure of the concrete [89,90]. Moreover, calcareous aggregates undergo severe processes of physical destruction above 800 °C due to the calcination of calcite [91]. This destruction can be observed in Figure 17, in which the regions with blue color indicate concrete with very low remaining compressive strength.

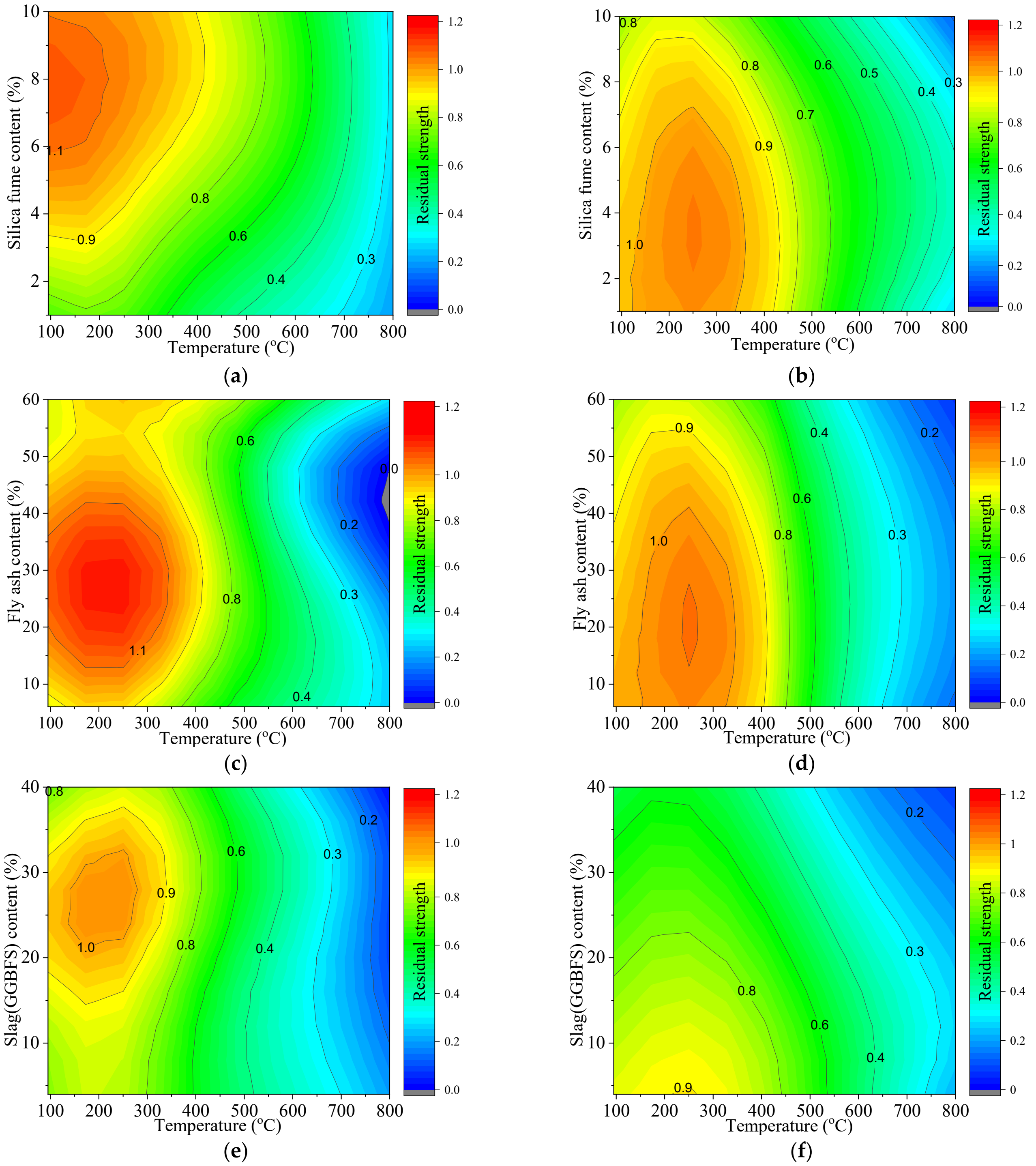

Figure 17. The influence of SCMs content in concrete with w/b of 0.6 on the residual compressive strength (**a**) Si-SF, (**b**) Ca-SF, (**c**) Si-FA, (**d**) Ca-FA, (**e**) Si-GGBFS, and (**f**) Ca-GGBFS.

Comparing the results of Figure 17a,b indicates that the optimum SCMs contents completely depend on the aggregate types along with other parameters, namely mix design. The optimum SF content for concrete with a w/b ratio of 0.6 containing siliceous aggregate is around 8%; while for concrete containing calcareous aggregate, it is about 3%. The same results were obtained in previous experimental tests [6,38,92,93]. The interactive effects of FA content and temperatures on the residual compressive strength of siliceous and calcareous concrete are presented in Figures 17c and 17d, respectively. For siliceous concrete, the higher residual strength occurs between 200 °C and 300 °C with 30% FA content. At temperatures above 300 °C, the relative compressive strength decreases continuously for all concrete mixes. For temperatures beyond 300 °C, the strength loss is fairly indifferent to FA concrete, as indicated by the red colour core in temperatures below 300 °C. In calcareous concrete, as shown in Figure 17d, the variation of FA content up to 40 % has no significant effect on the strength loss for temperatures below 400 °C. Regarding GGBFS concrete, Figure 17e shows that the siliceous concrete containing 20–35% GGBFS performs better than other concrete mixes at all temperatures. It can be seen from Figure 17f for calcareous concrete that compressive strength is reduced with increasing of the content of GGBFS at all temperatures. In addition, in the presence of GGBFS, the rate of strength loss was higher in calcareous concrete than in siliceous concrete. Overall, Figure 17 illustrates a slightly better behaviour of silicious aggregate. Nonetheless, the other parameters, such as silica type and its amount in the aggregate, porosity, moisture content, etc., are crucial for concrete specimens at high temperatures [94]. However, measuring these parameters is difficult and costly. This may be one of the reasons that available studies in the literature report only the type of aggregate. Therefore, considering these parameters (e.g., porosity and moisture content) in the ANN model was not feasible due to insufficient data. However, the current study considered the complex effect of various parameters and their interactions with each other on the residual compressive strength of concrete at high temperatures using the generalization ability of machine-learning approaches. The ability of the proposed network to predict the degradation of the compressive strength of concrete at high temperatures was proven. The results of the proposed network can be used to understand the effects of high temperature, concrete mix design, SCM types, test types, and aggregate classes on the thermal response of concrete.

4. Conclusions

The behaviour of concrete under high temperatures is complex and affected by several factors. The main purpose of this study was to predict the compressive strength of concrete when subjected to high temperatures. A total of 500 data points were gathered to establish the artificial neuron network (ANN) model to forecast the compressive strength of concrete exposed to high temperatures. Furthermore, a parametric study was conducted to evaluate the effects of input variables on the mechanical characteristics of concrete using the ANN model. Based on analyzing the prediction of the ANN model, the following conclusions were drawn:

1. A network consisting of one hidden layer within twelve neurons was established to estimate the compressive strength of concrete exposed to high temperatures. The network has a mean-squared error (MSE) of 0.004 and a correlation coefficient (R) of 0.966.
2. The database contained experimental test results from three common test protocols: transient temperature, steady-state temperature, and residual tests. It was found that the strength loss in transient tests is lower than in the steady-state and residual tests for all aggregate types.
3. A higher w/c ratio for both siliceous- and calcareous-aggregate concrete results in more strength loss after exposure to high temperatures.
4. The better thermal performance of silicious aggregates was observed in various concrete mixes containing different SCMs. Chemical reactions between quartz and $Ca(OH)_2$, as well as a higher C-S-H formation rate in siliceous aggregates, resulted in a stronger bond with cement paste rather than calcareous aggregates. However, the bond strength completely depends on the chemical composition of aggregates and SCMs.
5. For all concrete, regardless of SCM type and aggregate type, the maximum residual compressive strength is around 100–300 °C. This may be attributed to the possibility of steam curing resulting in additional hydration of unhydrated cement particles at temperatures 100–300 °C.

6. The optimum amount of SCMs depends on factors such as aggregate types, which are not fully studied experimentally, and the data lack exists. The optimum amount of SCMs may differ based on the aggregate type; for instance, the optimum silica fume (SF) content for concrete with a w/b ratio of 0.6 subjected to high temperatures is 8% and 3% for siliceous and calcareous concrete, respectively.
7. In siliceous-aggregate concrete, adding FA increases the relative compressive strength by over 15%. For calcareous aggregate and temperatures below 400 °C, adding FA results in a 10% higher strength. In calcareous concrete, FA replacement over 40% results in more strength loss at all temperatures. The residual compressive strength decreased continuously for slag (GGBFS)-containing silicious and calcareous concrete. However, the compressive strength reduction was more significant in GGBFS calcareous concrete.
8. To draw a general conclusion on the effects of different SCMs on the residual compressive strength of concrete, for siliceous concrete with a w/b ratio of 0.3 using Figures 13–16, the FA concrete shows better results, followed by GGBFS and silica fume.

Author Contributions: Conceptualization, S.R. and H.H.; methodology, S.R. and M.J.M.; software, S.R.; validation, S.R., M.J.M. and H.H.; formal analysis, S.R., M.J.M. and H.H.; investigation, S.R.; resources, S.R.; data curation, S.R; writing—original draft preparation S.R.; writing—review and editing, S.R., M.J.M. and H.H.; visualization, S.R., M.J.M. and H.H.; supervision, H.H.; project administration, H.H.; funding acquisition, H.H. All authors have read and agreed to the published version of the manuscript.

Funding: Natural Sciences and Engineering Research Council of Canada (NSERC).

Data Availability Statement: The data has been used in this study is presented in Appendix A.

Conflicts of Interest: The authors declare no conflict of interest.

Appendix A. Data Set Table

Table A1. Database that was collected to develop the ANN model.

	Paper	Temperature (°C)	Coarse-Aggregate Type	Coarse Aggregate (kg/m^3)	Fine Aggregate (kg/m^3)	SF%	FA%	GGBS%	Cement (kg/m^3)	Water (kg/m^3)	f_{cT}/f_{c20}	Test Method
1	[38]	200	S	1142	615	10	20	0	350	150	1.09	R
2		400	S	1142	615	10	20	0	350	150	0.94	R
3		600	S	1142	615	10	20	0	350	150	0.51	R
4		800	S	1142	615	10	20	0	350	150	0.19	R
5		200	S	1151	620	10	0	0	450	150	0.98	R
6		400	S	1151	620	10	0	0	450	150	0.87	R
7		600	S	1151	620	10	0	0	450	150	0.44	R
8		800	S	1151	620	10	0	0	450	150	0.16	R
9		200	S	1066	710	5	0	0	475	150	0.99	R
10		400	S	1066	710	5	0	0	475	150	0.93	R
11		600	S	1066	710	5	0	0	475	150	0.52	R
12		800	S	1066	710	5	0	0	475	150	0.21	R
13		200	S	1139	613	0	40	0	300	150	1.22	R
14		400	S	1139	613	0	40	0	300	150	1.04	R
15		600	S	1139	613	0	40	0	300	150	0.57	R
16		800	S	1139	613	0	40	0	300	150	0.30	R
17		200	S	1139	625	0	40	0	234	195	1.06	R
18		400	S	1139	625	0	40	0	234	195	0.84	R
19		600	S	1139	625	0	40	0	234	195	0.45	R
20		800	S	1139	625	0	40	0	234	195	0.18	R
21		200	S	1143	615	0	30	0	350	150	1.21	R
22		400	S	1143	615	0	30	0	350	150	0.98	R
23		600	S	1143	615	0	30	0	350	150	0.67	R
24		800	S	1143	615	0	30	0	350	150	0.32	R

Table A1. *Cont.*

	Paper	Temperature (°C)	Coarse-Aggregate Type	Coarse Aggregate (kg/m^3)	Fine Aggregate (kg/m^3)	SF%	FA%	GGBS%	Cement (kg/m^3)	Water (kg/m^3)	f_{cT}/f_{c20}	Test Method
25		200	S	1133	626	0	30	0	273	195	1.02	R
26		400	S	1133	626	0	30	0	273	195	0.86	R
27		600	S	1133	626	0	30	0	273	195	0.37	R
28		800	S	1133	626	0	30	0	273	195	0.16	R
29		200	S	1147	618	0	20	0	400	150	1.14	R
30		400	S	1147	618	0	20	0	400	150	0.96	R
31		600	S	1147	618	0	20	0	400	150	0.62	R
32		800	S	1147	618	0	20	0	400	150	0.28	R
33		200	S	1142	615	0	0	40	300	150	1.15	R
34		400	S	1142	615	0	0	40	300	150	0.99	R
35		600	S	1142	615	0	0	40	300	150	0.61	R
36		800	S	1142	615	0	0	40	300	150	0.29	R
37		200	S	1132	625	0	0	40	234	195	0.92	R
38		400	S	1132	625	0	0	40	234	195	0.81	R
39		600	S	1132	625	0	0	40	234	195	0.54	R
40		800	S	1132	625	0	0	40	234	195	0.20	R
41		200	S	1145	616	0	0	30	350	150	1.13	R
42		400	S	1145	616	0	0	30	350	150	0.97	R
43		600	S	1145	616	0	0	30	350	150	0.53	R
44		800	S	1145	616	0	0	30	350	150	0.24	R
45		200	S	1135	626	0	0	30	273	195	0.98	R
46		400	S	1135	626	0	0	30	273	195	0.85	R
47		600	S	1135	626	0	0	30	273	195	0.51	R
48		800	S	1135	626	0	0	30	273	195	0.21	R
49		200	S	927	758	0	0	0	500	150	0.96	R
50		400	S	927	758	0	0	0	500	150	0.89	R
51		600	S	927	758	0	0	0	500	150	0.58	R
52		800	S	927	758	0	0	0	500	150	0.24	R
53		200	S	917	768	0	0	0	390	195	0.93	R
54		400	S	917	768	0	0	0	390	195	0.74	R
55		600	S	917	768	0	0	0	390	195	0.30	R
56		800	S	917	768	0	0	0	390	195	0.10	R
57		100	S	955	634	7	15	0	452	170	0.76	TR
58		200	S	955	634	7	15	0	452	170	0.99	TR
59		300	S	955	634	7	15	0	452	170	1.00	TR
60		400	S	955	634	7	15	0	452	170	0.91	TR
61		500	S	955	634	7	15	0	452	170	0.72	TR
62		600	S	955	634	7	15	0	452	170	0.58	TR
63		700	S	955	634	7	15	0	452	170	0.47	TR
64		100	S	972	537	7	15	0	515	165	0.80	TR
65		200	S	972	537	7	15	0	515	165	0.93	TR
66		300	S	972	537	7	15	0	515	165	0.89	TR
67	[95]	400	S	972	537	7	15	0	515	165	0.74	TR
68		500	S	972	537	7	15	0	515	165	0.63	TR
69		600	S	972	537	7	15	0	515	165	0.59	TR
70		700	S	972	537	7	15	0	515	165	0.52	TR
71		100	S	919	793	0	10	0	344	176	0.78	TR
72		200	S	919	793	0	10	0	344	176	1.10	TR
73		300	S	919	793	0	10	0	344	176	1.10	TR
74		400	S	919	793	0	10	0	344	176	0.98	TR
75		500	S	919	793	0	10	0	344	176	0.75	TR
76		600	S	919	793	0	10	0	344	176	0.60	TR
77		700	S	919	793	0	10	0	344	176	0.44	TR

Table A1. *Cont.*

	Paper	Temperature (°C)	Coarse-Aggregate Type	Coarse Aggregate (kg/m^3)	Fine Aggregate (kg/m^3)	SF%	FA%	GGBS%	Cement (kg/m^3)	Water (kg/m^3)	f_{cT}/f_{c20}	Test Method
78	[6]	100	C	1168	615	10	0	0	450	149	0.84	R
79		200	C	1168	615	10	0	0	450	149	0.86	R
80		300	C	1168	615	10	0	0	450	149	0.69	R
81		600	C	1168	615	10	0	0	450	149	0.27	R
82		100	C	1115	653	6	0	0	441	164	0.85	R
83		200	C	1115	653	6	0	0	441	164	0.88	R
84		300	C	1115	653	6	0	0	441	164	0.76	R
85		600	C	1115	653	6	0	0	441	164	0.29	R
86		100	C	1168	615	6	0	0	465	149	0.85	R
87		200	C	1168	615	6	0	0	465	149	0.86	R
88		300	C	1168	615	6	0	0	465	149	0.71	R
89		600	C	1168	615	6	0	0	465	149	0.29	R
90		100	C	1030	687	0	0	0	430	172	0.87	R
91		200	C	1030	687	0	0	0	430	172	0.90	R
92		300	C	1030	687	0	0	0	430	172	0.75	R
93		600	C	1030	687	0	0	0	430	172	0.33	R
94		100	C	1168	615	0	0	0	495	149	0.85	R
95		200	C	1168	615	0	0	0	495	149	0.89	R
96		300	C	1168	615	0	0	0	495	149	0.73	R
97		600	C	1168	615	0	0	0	495	149	0.31	R
98	[39]	200	S	1143	615	0	60	0	180	135	1.09	R
99		400	S	1143	615	0	60	0	180	135	0.93	R
100		600	S	1143	615	0	60	0	180	135	0.57	R
101		200	S	1161	625	0	40	0	270	135	0.92	R
102		400	S	1161	625	0	40	0	270	135	0.88	R
103		600	S	1161	625	0	40	0	270	135	0.62	R
104		800	S	1161	625	0	40	0	270	135	0.23	R
105		200	S	1179	634	0	20	0	360	135	0.90	R
106		400	S	1179	634	0	20	0	360	135	0.85	R
107		600	S	1179	634	0	20	0	360	135	0.59	R
108		800	S	1179	634	0	20	0	360	135	0.28	R
109		200	S	1196	643	0	0	0	450	135	1.06	R
110		400	S	1196	643	0	0	0	450	135	0.81	R
111		600	S	1196	643	0	0	0	450	135	0.55	R
112		800	S	1196	643	0	0	0	450	135	0.28	R
113	[46]	250	S	1132	536	0	55	0	184.5	250	1.12	R
114		450	S	1132	536	0	55	0	184.5	250	0.97	R
115		650	S	1132	536	0	55	0	184.5	250	0.63	R
116		800	S	1132	536	0	55	0	184.5	250	0.26	R
117		250	S	1086	634	0	55	0	225	150	1.23	R
118		450	S	1086	634	0	55	0	225	150	0.99	R
119		650	S	1086	634	0	55	0	225	150	0.65	R
120		800	S	1086	634	0	55	0	225	150	0.27	R
121		250	S	1132	576	0	25	0	410	205	1.15	R
122		450	S	1132	576	0	25	0	307.5	205	0.86	R
123		650	S	1132	576	0	25	0	307.5	205	0.51	R
124		800	S	1132	576	0	25	0	307.5	205	0.27	R
125		250	S	1086	683	0	25	0	375	150	1.14	R
126		450	S	1086	683	0	25	0	375	150	0.86	R
127		650	S	1086	683	0	25	0	375	150	0.56	R
128		800	S	1086	683	0	25	0	375	150	0.30	R
129		250	S	1132	609	0	0	0	410	205	1.10	R
130		450	S	1132	609	0	0	0	410	205	0.86	R
131		650	S	1132	609	0	0	0	410	205	0.52	R
132		800	S	1132	609	0	0	0	410	205	0.24	R
133		250	S	1086	724	0	0	0	500	150	1.09	R
134		450	S	1086	724	0	0	0	500	150	0.83	R
135		650	S	1086	724	0	0	0	500	150	0.52	R
136		800	S	1086	724	0	0	0	500	150	0.21	R

Table A1. *Cont.*

	Paper	Temperature (°C)	Coarse-Aggregate Type	Coarse Aggregate (kg/m^3)	Fine Aggregate (kg/m^3)	SF%	FA%	GGBS%	Cement (kg/m^3)	Water (kg/m^3)	f_{cT}/f_{c20}	Test Method
137	[92]	100	LWA	601	730	10	0	0	387	202	0.75	R
138		400	LWA	601	730	10	0	0	387	202	0.39	R
139		800	LWA	601	730	10	0	0	387	202	0.16	R
140		100	LWA	601	730	5	0	0	408.5	202	1.04	R
141		400	LWA	601	730	5	0	0	408.5	202	0.90	R
142		800	LWA	601	730	5	0	0	408.5	202	0.33	R
143		100	LWA	602	729	0	0	0	430	199	0.99	R
144		400	LWA	602	729	0	0	0	430	199	0.79	R
145		800	LWA	602	729	0	0	0	430	199	0.28	R
146	[37]	95	C	1050	699	0	0	0	354	195	0.94	R
147		205	C	1050	699	0	0	0	354	195	0.84	R
148		315	C	1050	699	0	0	0	354	195	0.70	R
149		425	C	1050	699	0	0	0	354	195	0.62	R
150		535	C	1050	699	0	0	0	354	195	0.49	R
151		650	C	1050	699	0	0	0	354	195	0.34	R
152		95	S	1050	699	0	0	0	354	195	0.91	R
153		205	S	1050	699	0	0	0	354	195	0.82	R
154		315	S	1050	699	0	0	0	354	195	0.74	R
155		425	S	1050	699	0	0	0	354	195	0.62	R
156		535	S	1050	699	0	0	0	354	195	0.49	R
157		650	S	1050	699	0	0	0	354	195	0.35	R
158		95	S	1050	699	0	0	0	354	195	0.95	R
159		205	S	1050	699	0	0	0	354	195	0.87	R
160		315	S	1050	699	0	0	0	354	195	0.80	R
161		425	S	1050	699	0	0	0	354	195	0.70	R
162		535	S	1050	699	0	0	0	354	195	0.61	R
163		650	S	1050	699	0	0	0	354	195	0.54	R
164	[42]	100	C	1168	615	10	0	0	450	149	0.84	R
165		200	C	1168	615	10	0	0	450	149	0.85	R
166		300	C	1168	615	10	0	0	450	149	0.68	R
167		600	C	1168	615	10	0	0	450	149	0.27	R
168		100	C	1115	653	6	0	0	441	164	0.85	R
169		200	C	1115	653	6	0	0	441	164	0.88	R
170		300	C	1115	653	6	0	0	441	164	0.77	R
171		600	C	1115	653	6	0	0	441	164	0.29	R
172		100	C	1168	615	0	0	0	500	149	0.86	R
173		200	C	1168	615	0	0	0	500	149	0.88	R
174		300	C	1168	615	0	0	0	500	149	0.73	R
175		600	C	1168	615	0	0	0	500	149	0.31	R
176		100	C	1030	687	0	0	0	430	172	0.85	R
177		200	C	1030	687	0	0	0	430	172	0.88	R
178		300	C	1030	687	0	0	0	430	172	0.74	R
179		600	C	1030	687	0	0	0	430	172	0.33	R
180	[96]	150	LWA	369	777	0	0	0	426	192	0.98	R
181		300	LWA	369	777	0	0	0	426	192	0.97	R
182		450	LWA	369	777	0	0	0	426	192	0.73	R
183		600	LWA	369	777	0	0	0	426	192	0.44	R
184		150	LWA	585	777	0	0	0	426	192	0.96	R
185		300	LWA	585	777	0	0	0	426	192	1.01	R
186		450	LWA	585	777	0	0	0	426	192	0.72	R
187		600	LWA	585	777	0	0	0	426	192	0.45	R
188		150	LWA	547	777	0	0	0	426	192	0.91	R
189		300	LWA	547	777	0	0	0	426	192	1.00	R
190		450	LWA	547	777	0	0	0	426	192	0.82	R
191		600	LWA	547	777	0	0	0	426	192	0.49	R
192		150	C	1002	777	0	0	0	426	192	0.86	R
193		300	C	1002	777	0	0	0	426	192	0.92	R
194		450	C	1002	777	0	0	0	426	192	0.63	R
195		600	C	1002	777	0	0	0	426	192	0.33	R

Table A1. *Cont.*

	Paper	Temperature (°C)	Coarse-Aggregate Type	Coarse Aggregate (kg/m^3)	Fine Aggregate (kg/m^3)	SF%	FA%	GGBS%	Cement (kg/m^3)	Water (kg/m^3)	f_{cT}/f_{c20}	Test Method
196		100	LWA	676	687	0	0	0	432	155	0.76	TR
197		200	LWA	676	687	0	0	0	432	155	0.82	TR
198		300	LWA	676	687	0	0	0	432	155	0.99	TR
199		500	LWA	676	687	0	0	0	432	155	0.88	TR
200		700	LWA	676	687	0	0	0	432	155	0.90	TR
201		100	LWA	676	687	0	0	0	432	155	0.83	TR
202		200	LWA	676	687	0	0	0	432	155	0.94	TR
203		300	LWA	676	687	0	0	0	432	155	1.01	TR
204		500	LWA	676	687	0	0	0	432	155	0.94	TR
205		700	LWA	676	687	0	0	0	432	155	0.86	TR
206		100	LWA	676	687	0	0	0	432	155	0.84	SS
207		200	LWA	676	687	0	0	0	432	155	0.90	SS
208		300	LWA	676	687	0	0	0	432	155	0.95	SS
209	[45]	500	LWA	676	687	0	0	0	432	155	0.76	SS
210		700	LWA	676	687	0	0	0	432	155	0.62	SS
211		100	S	1071	692	0	0	0	470	165	0.66	TR
212		200	S	1071	692	0	0	0	470	165	0.79	TR
213		300	S	1071	692	0	0	0	470	165	0.96	TR
214		500	S	1071	692	0	0	0	470	165	0.72	TR
215		700	S	1071	692	0	0	0	470	165	0.11	TR
216		100	S	1071	692	0	0	0	470	165	0.69	TR
217		200	S	1071	692	0	0	0	470	165	0.72	TR
218		300	S	1071	692	0	0	0	470	165	0.93	TR
219		500	S	1071	692	0	0	0	470	165	0.68	TR
220		700	S	1071	692	0	0	0	470	165	0.38	TR
221		300	S	1071	692	0	0	0	470	165	0.88	SS
222		500	S	1071	692	0	0	0	470	165	0.59	SS
223		700	S	1071	692	0	0	0	470	165	0.27	SS
224		204	C	1085	855	0	0	0	237	130	0.88	SS
225		482	C	1085	855	0	0	0	237	130	0.79	SS
226		704	C	1085	855	0	0	0	237	130	0.63	SS
227		871	C	1085	855	0	0	0	237	130	0.08	SS
228		204	C	1085	855	0	0	0	237	130	0.98	TR
229		482	C	1085	855	0	0	0	237	130	0.99	TR
230		704	C	1085	855	0	0	0	237	130	0.88	TR
231		204	C	1085	855	0	0	0	237	130	0.79	R
232		482	C	1085	855	0	0	0	237	130	0.49	R
233		704	C	1085	855	0	0	0	237	130	0.35	R
234		760	C	1085	855	0	0	0	237	130	0.32	R
235		204	C	955	870	0	0	0	317	134	0.86	SS
236		482	C	955	870	0	0	0	317	134	0.78	SS
237		704	C	955	870	0	0	0	317	134	0.78	SS
238		871	C	955	870	0	0	0	317	134	0.14	SS
239		204	C	955	870	0	0	0	317	134	0.98	TR
240		482	C	955	870	0	0	0	317	134	0.96	TR
241		704	C	955	870	0	0	0	317	134	0.96	TR
242	[41]	204	C	955	870	0	0	0	317	134	0.79	R
243		482	C	955	870	0	0	0	317	134	0.49	R
244		704	C	955	870	0	0	0	317	134	0.35	R
245		760	C	955	870	0	0	0	317	134	0.32	R
246		204	S	1080	855	0	0	0	249	127	0.91	SS
247		482	S	1080	855	0	0	0	249	127	0.73	SS
248		704	S	1080	855	0	0	0	249	127	0.25	SS
249		871	S	1080	855	0	0	0	249	127	0.22	SS
250		204	S	1080	855	0	0	0	249	127	1.05	TR
251		482	S	1080	855	0	0	0	249	127	0.93	TR
252		649	S	1080	855	0	0	0	249	127	0.57	TR
253		204	S	1080	855	0	0	0	249	127	0.86	R
254		482	S	1080	855	0	0	0	249	127	0.58	R
255		704	S	1080	855	0	0	0	249	127	0.15	R
256		204	S	1000	880	0	0	0	330	132	0.90	SS
257		482	S	1000	880	0	0	0	330	132	0.73	SS
258		704	S	1000	880	0	0	0	330	132	0.26	SS
259		871	S	1000	880	0	0	0	330	132	0.13	SS
260		204	S	1000	880	0	0	0	330	132	0.99	TR

Table A1. *Cont.*

	Paper	Temperature (°C)	Coarse-Aggregate Type	Coarse Aggregate (kg/m^3)	Fine Aggregate (kg/m^3)	SF%	FA%	GGBS%	Cement (kg/m^3)	Water (kg/m^3)	f_{cT}/f_{c20}	Test Method
261		482	S	1000	880	0	0	0	330	132	0.71	TR
262		649	S	1000	880	0	0	0	330	132	0.41	TR
263		204	S	1000	880	0	0	0	330	132	0.89	R
264		482	S	1000	880	0	0	0	330	132	0.57	R
265		649	S	1000	880	0	0	0	330	132	0.17	R
266		204	LWA	493	762	0	0	0	264	206	0.95	SS
267		482	LWA	493	762	0	0	0	264	206	0.83	SS
268		704	LWA	493	762	0	0	0	264	206	0.69	SS
269		871	LWA	493	762	0	0	0	264	206	0.23	SS
270		204	LWA	493	762	0	0	0	264	206	0.94	TR
271		482	LWA	493	762	0	0	0	264	206	0.85	TR
272		704	LWA	493	762	0	0	0	264	206	0.70	TR
273		204	LWA	493	762	0	0	0	264	206	0.88	R
274		482	LWA	493	762	0	0	0	264	206	0.63	R
275		704	LWA	493	762	0	0	0	264	206	0.44	R
276		871	LWA	493	762	0	0	0	264	206	0.12	R
277		204	LWA	482	678	0	0	0	350	206	0.95	SS
278		482	LWA	482	678	0	0	0	350	206	0.83	SS
279		704	LWA	482	678	0	0	0	350	206	0.69	SS
280		871	LWA	482	678	0	0	0	350	206	0.23	SS
281		204	LWA	482	678	0	0	0	350	206	0.94	TR
282		482	LWA	482	678	0	0	0	350	206	0.85	TR
283		704	LWA	482	678	0	0	0	350	206	0.70	TR
284		204	LWA	482	678	0	0	0	350	206	0.91	R
285		482	LWA	482	678	0	0	0	350	206	0.54	R
286		704	LWA	482	678	0	0	0	350	206	0.39	R
287		871	LWA	482	678	0	0	0	350	206	0.16	R
288		100	C	1095.3	794.7	0	30	0	210	180	0.95	R
289		300	C	1095.3	794.7	0	30	0	210	180	0.92	R
290		600	C	1095.3	794.7	0	30	0	210	180	0.41	R
291		750	C	1095.3	794.7	0	30	0	210	180	0.19	R
292		100	S	1040.4	807.6	0	30	0	210	180	1.19	R
293		300	S	1040.4	807.6	0	30	0	210	180	1.32	R
294		600	S	1040.4	807.6	0	30	0	210	180	0.49	R
295		750	S	1040.4	807.6	0	30	0	210	180	0.22	R
296		100	C	1095.3	794.7	0	30	0	210	180	1.05	R
297		300	C	1095.3	794.7	0	30	0	210	180	1.06	R
298		600	C	1095.3	794.7	0	30	0	210	180	0.40	R
299		750	C	1095.3	794.7	0	30	0	210	180	0.07	R
300		100	S	1040.4	807.6	0	30	0	210	180	0.97	R
301		300	S	1040.4	807.6	0	30	0	210	180	1.16	R
302		600	S	1040.4	807.6	0	30	0	210	180	0.32	R
303		750	S	1040.4	807.6	0	30	0	210	180	0.12	R
304		100	C	1095.3	794.7	0	30	0	210	180	1.03	R
305		300	C	1095.3	794.7	0	30	0	210	180	1.11	R
306	[43]	600	C	1095.3	794.7	0	30	0	210	180	0.34	R
307		750	C	1095.3	794.7	0	30	0	210	180	0.24	R
308		100	S	1040.4	807.6	0	30	0	210	180	1.24	R
309		300	S	1040.4	807.6	0	30	0	210	180	1.24	R
310		600	S	1040.4	807.6	0	30	0	210	180	0.47	R
311		750	S	1040.4	807.6	0	30	0	210	180	0.25	R
312		100	C	1095.3	794.7	0	10	0	270	180	0.91	R
313		300	C	1095.3	794.7	0	10	0	270	180	0.92	R
314		600	C	1095.3	794.7	0	10	0	270	180	0.50	R
315		750	C	1095.3	794.7	0	10	0	270	180	0.23	R
316		100	S	1040.4	807.6	0	10	0	270	180	0.95	R
317		300	S	1040.4	807.6	0	10	0	270	180	1.06	R
318		600	S	1040.4	807.6	0	10	0	270	180	0.50	R
319		750	S	1040.4	807.6	0	10	0	270	180	0.25	R
320		100	C	1095.3	794.7	0	10	0	270	180	1.06	R
321		300	C	1095.3	794.7	0	10	0	270	180	1.14	R
322		600	C	1095.3	794.7	0	10	0	270	180	0.44	R
323		750	C	1095.3	794.7	0	10	0	270	180	0.13	R
324		100	S	1040.4	807.6	0	10	0	270	180	1.13	R
325		300	S	1040.4	807.6	0	10	0	270	180	1.32	R

Table A1. *Cont.*

	Paper	Temperature (°C)	Coarse-Aggregate Type	Coarse Aggregate (kg/m^3)	Fine Aggregate (kg/m^3)	SF%	FA%	GGBS%	Cement (kg/m^3)	Water (kg/m^3)	f_{cT}/f_{c20}	Test Method
326		600	S	1040.4	807.6	0	10	0	270	180	0.40	R
327		750	S	1040.4	807.6	0	10	0	270	180	0.15	R
328		100	C	1095.3	794.7	0	10	0	270	180	1.08	R
329		300	C	1095.3	794.7	0	10	0	270	180	1.11	R
330		600	C	1095.3	794.7	0	10	0	270	180	0.42	R
331		750	C	1095.3	794.7	0	10	0	270	180	0.15	R
332		100	S	1040.4	807.6	0	10	0	270	180	1.13	R
333		300	S	1040.4	807.6	0	10	0	270	180	1.37	R
334		600	S	1040.4	807.6	0	10	0	270	180	0.45	R
335		750	S	1040.4	807.6	0	10	0	270	180	0.70	R
336		100	C	1095.3	794.7	0	0	0	300	180	0.99	R
337		300	C	1095.3	794.7	0	0	0	300	180	0.93	R
338		600	C	1095.3	794.7	0	0	0	300	180	0.52	R
339		750	C	1095.3	794.7	0	0	0	300	180	0.23	R
340		100	S	1040.4	807.6	0	0	0	300	180	0.89	R
341		300	S	1040.4	807.6	0	0	0	300	180	1.05	R
342		600	S	1040.4	807.6	0	0	0	300	180	0.48	R
343		750	S	1040.4	807.6	0	0	0	300	180	0.25	R
344		200	C	1200	600	0	0	0	400	200	0.94	R
345		400	C	1200	600	0	0	0	400	200	0.84	R
346		600	C	1200	600	0	0	0	400	200	0.56	R
347		200	S	1200	600	0	0	0	400	200	0.96	R
348	[44]	400	S	1200	600	0	0	0	400	200	0.83	R
349		600	S	1200	600	0	0	0	400	200	0.61	R
350		200	S	1200	600	0	0	0	400	200	0.89	R
351		400	S	1200	600	0	0	0	400	200	0.81	R
352		600	S	1200	600	0	0	0	400	200	0.63	R
353		100	C	845.8	733.6	10	0	0	595.5	133	0.82	R
354		100	C	845.8	733.6	10	0	0	595.5	133	0.87	R
355		100	C	845.8	733.6	10	0	0	595.5	133	0.93	R
356		200	C	845.8	733.6	10	0	0	595.5	133	1.00	R
357		200	C	845.8	733.6	10	0	0	595.5	133	0.95	R
358		200	C	845.8	733.6	10	0	0	595.5	133	0.94	R
359		300	C	845.8	733.6	10	0	0	595.5	133	0.90	R
360		300	C	845.8	733.6	10	0	0	595.5	133	0.83	R
361		300	C	845.8	733.6	10	0	0	595.5	133	0.89	R
362		100	C	845.8	733.6	10	0	0	595.9	198.6	0.89	R
363		100	C	845.8	733.6	10	0	0	595.9	198.6	0.90	R
364		100	C	845.8	733.6	10	0	0	595.9	198.6	0.82	R
365		200	C	845.8	733.6	10	0	0	595.9	198.6	0.77	R
366		200	C	845.8	733.6	10	0	0	595.9	198.6	0.79	R
367		200	C	845.8	733.6	10	0	0	595.9	198.6	0.81	R
368		300	C	845.8	733.6	10	0	0	595.9	198.6	0.67	R
369		100	C	846	734	10	0	0	596	133	0.77	TR
370		100	C	846	734	10	0	0	596	133	0.76	TR
371	[40]	100	C	846	734	10	0	0	596	133	0.85	TR
372		100	C	846	734	10	0	0	596	133	0.81	TR
373		100	C	846	734	10	0	0	596	133	0.73	TR
374		200	C	846	734	10	0	0	596	133	0.77	TR
375		200	C	846	734	10	0	0	596	133	0.82	TR
376		200	C	846	734	10	0	0	596	133	0.74	TR
377		300	C	846	734	10	0	0	596	133	0.79	TR
378		300	C	846	734	10	0	0	596	133	0.79	TR
379		300	C	846	734	10	0	0	596	133	0.88	TR
380		450	C	846	734	10	0	0	596	133	0.81	TR
381		450	C	846	734	10	0	0	596	133	0.76	TR
382		450	C	846	734	10	0	0	596	133	0.82	TR
383		600	C	846	734	10	0	0	596	133	0.73	TR
384		600	C	846	734	10	0	0	596	133	0.67	TR
385		600	C	846	734	10	0	0	596	133	0.59	TR
386		100	C	846	734	10	0	0	596	199	0.69	TR
387		100	C	846	734	10	0	0	596	199	0.60	TR
388		100	C	846	734	10	0	0	596	199	0.72	TR
389		200	C	846	734	10	0	0	596	199	0.75	TR
390		200	C	846	734	10	0	0	596	199	0.74	TR

Table A1. *Cont.*

	Paper	Temperature (°C)	Coarse-Aggregate Type	Coarse Aggregate (kg/m^3)	Fine Aggregate (kg/m^3)	SF%	FA%	GGBS%	Cement (kg/m^3)	Water (kg/m^3)	f_{cT}/f_{c20}	Test Method
391		200	C	846	734	10	0	0	596	199	0.73	TR
392		300	C	846	734	10	0	0	596	199	0.78	TR
393		300	C	846	734	10	0	0	596	199	0.71	TR
394		300	C	846	734	10	0	0	596	199	0.81	TR
395		450	C	846	734	10	0	0	596	199	0.70	TR
396		450	C	846	734	10	0	0	596	199	0.77	TR
397		100	C	846	734	10	0	0	596	133	0.71	SS
398		100	C	846	734	10	0	0	596	133	0.63	SS
399		100	C	846	734	10	0	0	596	133	0.71	SS
400		200	C	846	734	10	0	0	596	133	0.81	SS
401		200	C	846	734	10	0	0	596	133	0.63	SS
402		200	C	846	734	10	0	0	596	133	0.78	SS
403		300	C	846	734	10	0	0	596	133	0.71	SS
404		300	C	846	734	10	0	0	596	133	0.95	SS
405		300	C	846	734	10	0	0	596	133	0.70	SS
406		300	C	846	734	10	0	0	596	133	0.80	SS
407		100	C	846	734	10	0	0	596	199	0.66	SS
408		100	C	846	734	10	0	0	596	199	0.64	SS
409		100	C	846	734	10	0	0	596	199	0.62	SS
410		200	C	846	734	10	0	0	596	199	0.69	SS
411		200	C	846	734	10	0	0	596	199	0.71	SS
412		200	C	846	734	10	0	0	596	199	0.68	SS
413		300	C	846	734	10	0	0	596	199	0.82	SS
414		300	C	846	734	10	0	0	596	199	0.63	SS
415		300	C	846	734	10	0	0	596	199	0.78	SS
416		450	C	846	734	10	0	0	596	199	0.64	SS
417		450	C	846	734	10	0	0	596	199	0.72	SS
418		300	C	845.8	733.6	0	0	0	661.6	198.6	0.64	R
419		300	C	845.8	733.6	0	0	0	661.6	198.6	0.70	R
420		450	C	845.8	733.6	0	0	0	661.6	198.6	0.47	R
421		450	C	845.8	733.6	0	0	0	661.6	198.6	0.50	R
422		450	C	845.8	733.6	0	0	0	661.6	198.6	0.47	R
423		100	C	845.8	733.6	0	0	0	661.6	198.6	0.77	R
424		100	C	845.8	733.6	0	0	0	661.6	198.6	0.74	R
425		100	C	845.8	733.6	0	0	0	661.6	198.6	0.78	R
426		200	C	845.8	733.6	0	0	0	661.6	198.6	0.79	R
427		200	C	845.8	733.6	0	0	0	661.6	198.6	0.70	R
428		200	C	845.8	733.6	0	0	0	661.6	198.6	0.75	R
429		300	C	845.8	733.6	0	0	0	661.6	198.6	0.74	R
430		300	C	853.8	868.2	0	0	0	376.4	213	0.76	R
431		300	C	853.8	868.2	0	0	0	376.4	213	0.71	R
432	[40]	450	C	853.8	868.2	0	0	0	376.4	213	0.55	R
433		450	C	853.8	868.2	0	0	0	376.4	213	0.49	R
434		450	C	853.8	868.2	0	0	0	376.4	213	0.51	R
435		100	C	853.8	868.2	0	0	0	376.4	213	0.70	R
436		100	C	853.8	868.2	0	0	0	376.4	213	0.69	R
437		100	C	853.8	868.2	0	0	0	376.4	213	0.72	R
438		200	C	853.8	868.2	0	0	0	376.4	213	0.77	R
439		200	C	853.8	868.2	0	0	0	376.4	213	0.72	R
440		200	C	853.8	868.2	0	0	0	376.4	213	0.72	R
441		300	C	853.8	868.2	0	0	0	376.4	213	0.69	R
442		300	C	853.8	868.2	0	0	0	376.4	213	0.66	R
443		300	C	853.8	868.2	0	0	0	376.4	213	0.65	R
444		450	C	853.8	868.2	0	0	0	376.4	213	0.53	R
445		450	C	853.8	868.2	0	0	0	376.4	213	0.50	R
446		450	C	853.8	868.2	0	0	0	376.4	213	0.48	R
447		100	C	846	734	0	0	0	662	194	0.70	TR
448		100	C	846	734	0	0	0	662	194	0.67	TR
449		100	C	846	734	0	0	0	662	194	0.67	TR
450		200	C	846	734	0	0	0	662	194	0.71	TR
451		200	C	846	734	0	0	0	662	194	0.71	TR
452		200	C	846	734	0	0	0	662	194	0.78	TR
453		300	C	846	734	0	0	0	662	194	0.72	TR
454		300	C	846	734	0	0	0	662	194	0.76	TR
455		300	C	846	734	0	0	0	662	194	0.79	TR

Table A1. *Cont.*

	Paper	Temperature (°C)	Coarse-Aggregate Type	Coarse Aggregate (kg/m^3)	Fine Aggregate (kg/m^3)	SF%	FA%	GGBS%	Cement (kg/m^3)	Water (kg/m^3)	f_{cT}/f_{c20}	Test Method
456		450	C	846	734	0	0	0	662	194	0.71	TR
457		450	C	846	734	0	0	0	662	194	0.85	TR
458		450	C	846	734	0	0	0	662	194	0.71	TR
459		100	C	854	868	0	0	0	376	213	0.74	TR
460		100	C	854	868	0	0	0	376	213	0.72	TR
461		100	C	854	868	0	0	0	376	213	0.72	TR
462		200	C	854	868	0	0	0	376	213	0.77	TR
463		200	C	854	868	0	0	0	376	213	0.81	TR
464		200	C	854	868	0	0	0	376	213	0.76	TR
465		300	C	854	868	0	0	0	376	213	0.77	TR
466		300	C	854	868	0	0	0	376	213	0.89	TR
467		300	C	854	868	0	0	0	376	213	0.79	TR
468		450	C	854	868	0	0	0	376	213	0.85	TR
469		450	C	854	868	0	0	0	376	213	0.75	TR
470		450	C	854	868	0	0	0	376	213	0.72	TR
471		600	C	854	868	0	0	0	376	213	0.46	TR
472		600	C	854	868	0	0	0	376	213	0.44	TR
473		600	C	854	868	0	0	0	376	213	0.45	TR
474		450	C	846	734	0	0	0	662	194	0.58	SS
475		100	C	846	734	0	0	0	662	194	0.67	SS
476		100	C	846	734	0	0	0	662	194	0.69	SS
477		100	C	846	734	0	0	0	662	194	0.71	SS
478		200	C	846	734	0	0	0	662	194	0.67	SS
479		200	C	846	734	0	0	0	662	194	0.79	SS
480		200	C	846	734	0	0	0	662	194	0.65	SS
481		300	C	846	734	0	0	0	662	194	0.92	SS
482		300	C	846	734	0	0	0	662	194	0.88	SS
483		300	C	854	868	0	0	0	376	213	0.70	SS
484	[40]	450	C	854	868	0	0	0	376	213	0.69	SS
485		450	C	854	868	0	0	0	376	213	0.82	SS
486		450	C	854	868	0	0	0	376	213	0.75	SS
487		100	C	854	868	0	0	0	376	213	0.75	SS
488		100	C	854	868	0	0	0	376	213	0.73	SS
489		100	C	854	868	0	0	0	376	213	0.71	SS
490		200	C	854	868	0	0	0	376	213	0.79	SS
491		200	C	854	868	0	0	0	376	213	0.71	SS
492		200	C	854	868	0	0	0	376	213	0.75	SS
493		300	C	854	868	0	0	0	376	213	0.74	SS
494		300	C	854	868	0	0	0	376	213	0.79	SS
495		300	C	854	868	0	0	0	376	213	0.73	SS
496		450	C	854	868	0	0	0	376	213	0.62	SS
497		450	C	854	868	0	0	0	376	213	0.73	SS
498		450	C	854	868	0	0	0	376	213	0.71	SS
499		600	C	854	868	0	0	0	376	213	0.30	SS
500		600	C	854	868	0	0	0	376	213	0.34	SS

References

1. Toutanji, H.A.; Bayasi, Z. Effect of curing procedures on properties of silica fume concrete. *Cem. Concr. Res.* **1999**, *29*, 497–501. [CrossRef]
2. Yazıcı, Ş.; Sezer, G.İ.; Şengül, H. The effect of high temperature on the compressive strength of mortars. *Constr. Build. Mater.* **2012**, *35*, 97–100. [CrossRef]
3. Ramzi, S.; Hajiloo, H. The Effects of Supplementary Cementitious Materials (SCMs) on the Residual Mechanical Properties of Concrete after Exposure to High Temperatures. *Buildings* **2023**, *13*, 103. [CrossRef]
4. Lothenbach, B.; Scrivener, K.; Hooton, R.D. Supplementary cementitious materials. *Cem. Concr. Res.* **2011**, *41*, 1244–1256. [CrossRef]
5. Sivakrishna, A.; Adesina, A.; Awoyera, P.; Kumar, K.R. Green concrete: A review of recent developments. *Mater. Today Proc.* **2020**, *27*, 54–58. [CrossRef]
6. Behnood, A.; Ziari, H. Effects of silica fume addition and water to cement ratio on the properties of high-strength concrete after exposure to high temperatures. *Cem. Concr. Compos.* **2008**, *30*, 106–112. [CrossRef]

7. Ibrahim, W.M.W.; Abdullah, M.M.A.B.; Ahmad, R.; Sandu, A.V.; Vizureanu, P.; Benjeddou, O.; Rahim, A.; Ibrahim, M.; Sauffi, A.S. Chemical distributions of different sodium hydroxide molarities on fly ash/dolomite-based geopolymer. *Materials* **2022**, *15*, 6163. [CrossRef]
8. Supit, S.W.; Shaikh, F.U.; Sarker, P.K. Effect of ultrafine fly ash on mechanical properties of high volume fly ash mortar. *Constr. Build. Mater.* **2014**, *51*, 278–286. [CrossRef]
9. Moon, G.D.; Oh, S.; Choi, Y.C. Effects of the physicochemical properties of fly ash on the compressive strength of high-volume fly ash mortar. *Constr. Build. Mater.* **2016**, *124*, 1072–1080. [CrossRef]
10. Onn, C.C.; Mo, K.H.; Radwan, M.K.H.; Liew, W.H.; Ng, C.G.; Yusoff, S. Strength, Carbon Footprint and Cost Considerations of Mortar Blends with High Volume Ground Granulated Blast Furnace Slag. *Sustainability* **2019**, *11*, 7194. [CrossRef]
11. Chidiac, S.; Panesar, D. Evolution of mechanical properties of concrete containing ground granulated blast furnace slag and effects on the scaling resistance test at 28 days. *Cem. Concr. Compos.* **2008**, *30*, 63–71. [CrossRef]
12. Nadeem, A.; Memon, S.A.; Lo, T.Y. Qualitative and quantitative analysis and identification of flaws in the microstructure of fly ash and metakaolin blended high performance concrete after exposure to elevated temperatures. *Constr. Build. Mater.* **2013**, *38*, 731–741. [CrossRef]
13. Mukherjee, A.; Biswas, S.N. Artificial neural networks in prediction of mechanical behavior of concrete at high temperature. *Nucl. Eng. Des.* **1997**, *178*, 1–11. [CrossRef]
14. Tang, Y.; Wang, Y.; Wu, D.; Liu, Z.; Zhang, H.; Zhu, M.; Chen, Z.; Sun, J.; Wang, X. An experimental investigation and machine learning-based prediction for seismic performance of steel tubular column filled with recycled aggregate concrete. *Rev. Adv. Mater. Sci.* **2022**, *61*, 849–872. [CrossRef]
15. Asteris, P.G.; Skentou, A.D.; Bardhan, A.; Samui, P.; Pilakoutas, K. Predicting concrete compressive strength using hybrid ensembling of surrogate machine learning models. *Cem. Concr. Res.* **2021**, *145*, 106449. [CrossRef]
16. Ashteyat, A.M.; Ismeik, M. Predicting residual compressive strength of self-compacted concrete under various temperatures and relative humidity conditions by artificial neural networks. *Comput. Concr.* **2018**, *21*, 47–54.
17. Vanluchene, R.D.; Sun, R. Neural networks in structural engineering. *Comput.-Aided Civ. Infrastruct. Eng.* **1990**, *5*, 207–215. [CrossRef]
18. Moradi, M.; Khaleghi, M.; Salimi, J.; Farhangi, V.; Ramezanianpour, A. Predicting the compressive strength of concrete containing metakaolin with different properties using ANN. *Measurement* **2021**, *183*, 109790. [CrossRef]
19. Özcan, F.; Atiş, C.D.; Karahan, O.; Uncuoğlu, E.; Tanyildizi, H. Comparison of artificial neural network and fuzzy logic models for prediction of long-term compressive strength of silica fume concrete. *Adv. Eng. Softw.* **2009**, *40*, 856–863. [CrossRef]
20. Tang, Y.; Huang, Z.; Chen, Z.; Chen, M.; Zhou, H.; Zhang, H.; Sun, J. Novel visual crack width measurement based on backbone double-scale features for improved detection automation. *Eng. Struct.* **2023**, *274*, 115158. [CrossRef]
21. Behnood, A.; Golafshani, E.M. Predicting the compressive strength of silica fume concrete using hybrid artificial neural network with multi-objective grey wolves. *J. Clean. Prod.* **2018**, *202*, 54–64. [CrossRef]
22. Atici, U. Prediction of the strength of mineral admixture concrete using multivariable regression analysis and an artificial neural network. *Expert Syst. Appl.* **2011**, *38*, 9609–9618. [CrossRef]
23. Chopra, P.; Sharma, R.K.; Kumar, M. Prediction of compressive strength of concrete using artificial neural network and genetic programming. *Adv. Mater. Sci. Eng.* **2016**, *2016*, 7648467. [CrossRef]
24. Boğa, A.R.; Öztürk, M.; Topçu, I.B. Using ANN and ANFIS to predict the mechanical and chloride permeability properties of concrete containing GGBFS and CNI. *Compos. Part B Eng.* **2013**, *45*, 688–696. [CrossRef]
25. Ahmad, A.; Ostrowski, K.A.; Maślak, M.; Farooq, F.; Mehmood, I.; Nafees, A. Comparative Study of Supervised Machine Learning Algorithms for Predicting the Compressive Strength of Concrete at High Temperature. *Materials* **2021**, *14*, 4222. [CrossRef] [PubMed]
26. Anderberg, Y.; Thelandersson, S. *Stress and Deformation Characteristics of Concrete at High Temperatures: Experimental Investigation and Material Behaviour Model*; Lund Institute of Technology: Lund, Sweden, 1976.
27. Abbas, H.; Al-Salloum, Y.A.; Elsanadedy, H.M.; Almusallam, T.H. ANN models for prediction of residual strength of HSC after exposure to elevated temperature. *Fire Saf. J.* **2019**, *106*, 13–28. [CrossRef]
28. Moradi, M.; Daneshvar, K.; Ghazi-Nader, D.; Hajiloo, H. The prediction of fire performance of concrete-filled steel tubes (CFST) using artificial neural network. *Thin-Walled Struct.* **2021**, *161*, 107499. [CrossRef]
29. Öztaş, A.; Pala, M.; Özbay, E.; Kanca, E.; Caglar, N.; Bhatti, M.A. Predicting the compressive strength and slump of high strength concrete using neural network. *Constr. Build. Mater.* **2006**, *20*, 769–775. [CrossRef]
30. Haykin, S.; Lippmann, R. Neural networks, a comprehensive foundation. *Int. J. Neural Syst.* **1994**, *5*, 363–364.
31. Topçu, İ.B.; Sarıdemir, M. Prediction of rubberized concrete properties using artificial neural network and fuzzy logic. *Constr. Build. Mater.* **2008**, *22*, 532–540. [CrossRef]
32. Mansour, M.Y.; Dicleli, M.; Lee, J.-Y.; Zhang, J. Predicting the shear strength of reinforced concrete beams using artificial neural networks. *Eng. Struct.* **2004**, *26*, 781–799. [CrossRef]
33. Demir, F. Prediction of elastic modulus of normal and high strength concrete by artificial neural networks. *Constr. Build. Mater.* **2008**, *22*, 1428–1435. [CrossRef]
34. Çelik, Ö.; Teke, A.; Yıldırım, H.B. The optimized artificial neural network model with Levenberg–Marquardt algorithm for global solar radiation estimation in Eastern Mediterranean Region of Turkey. *J. Clean. Prod.* **2016**, *116*, 1–12. [CrossRef]

35. Zhang, J.-R.; Zhang, J.; Lok, T.-M.; Lyu, M.R. A hybrid particle swarm optimization–back-propagation algorithm for feedforward neural network training. *Appl. Math. Comput.* **2007**, *185*, 1026–1037. [CrossRef]
36. Silva, F.A.N.; Delgado, J.M.P.Q.; Cavalcanti, R.S.; Azevedo, A.C.; Guimarães, A.S.; Lima, A.G.B. Use of Nondestructive Testing of Ultrasound and Artificial Neural Networks to Estimate Compressive Strength of Concrete. *Buildings* **2021**, *11*, 44. [CrossRef]
37. Tufail, M.; Shahzada, K.; Gencturk, B.; Wei, J. Effect of elevated temperature on mechanical properties of limestone, quartzite and granite concrete. *Int. J. Concr. Struct. Mater.* **2017**, *11*, 17–28. [CrossRef]
38. Poon, C.-S.; Azhar, S.; Anson, M.; Wong, Y.-L. Comparison of the strength and durability performance of normal- and high-strength pozzolanic concretes at elevated temperatures. *Cem. Concr. Res.* **2001**, *31*, 1291–1300. [CrossRef]
39. Nadeem, A.; Memon, S.A.; Lo, T.Y. The performance of fly ash and metakaolin concrete at elevated temperatures. *Constr. Build. Mater.* **2014**, *62*, 67–76. [CrossRef]
40. Phan, L.T.; Carino, N.J. Effects of Test Conditions and Mixture Proportions on Behavior of High-Strength Concrete Exposed to High Temperatures. *Mater. J.* **2002**, *99*, 54–56.
41. Abrams, M.S. Compressive strength of concrete at temperatures to 1600F. *Spec. Publ.* **1971**, *25*, 33–58.
42. Ghandehari, M.; Behnood, A.; Khanzadi, M. Residual mechanical properties of high-strength concretes after exposure to elevated temperatures. *J. Mater. Civ. Eng.* **2010**, *22*, 59–64. [CrossRef]
43. Savva, A.; Manita, P.; Sideris, K. Influence of elevated temperatures on the mechanical properties of blended cement concretes prepared with limestone and siliceous aggregates. *Cem. Concr. Compos.* **2005**, *27*, 239–248. [CrossRef]
44. Masood, A.; Shariq, M.; Alam, M.M.; Ahmad, T.; Beg, A. Effect of Elevated Temperature on the Residual Properties of Quartzite, Granite and Basalt Aggregate Concrete. *J. Inst. Eng. (India) Ser. A* **2018**, *99*, 485–494. [CrossRef]
45. Yoon, M.; Kim, G.; Choe, G.C.; Lee, Y.; Lee, T. Effect of coarse aggregate type and loading level on the high temperature properties of concrete. *Constr. Build. Mater.* **2015**, *78*, 26–33. [CrossRef]
46. Xu, Y.; Wong, Y.L.; Poon, C.S.; Anson, M. Influence of PFA on cracking of concrete and cement paste after exposure to high temperatures. *Cem. Concr. Res.* **2003**, *33*, 2009–2016. [CrossRef]
47. Kim, S.S.; Qudoos, A.; Jakhrani, S.H.; Lee, J.B.; Kim, H.G. Influence of coarse aggregates and Silica Fume on the mechanical properties, durability, and microstructure of concrete. *Materials* **2019**, *12*, 3324. [CrossRef]
48. Pliya, P.; Cree, D.; Hajiloo, H.; Beaucour, A.-L.; Green, M.F.; Noumowé, A. High-strength concrete containing recycled coarse aggregate subjected to elevated temperatures. *Fire Technol.* **2019**, *55*, 1477–1494. [CrossRef]
49. Elsanadedy, H.M. Residual compressive strength of high-strength concrete exposed to elevated temperatures. *Adv. Mater. Sci. Eng.* **2019**, *2019*, 6039571. [CrossRef]
50. Gupta, T.; Patel, K.; Siddique, S.; Sharma, R.K.; Chaudhary, S. Prediction of mechanical properties of rubberised concrete exposed to elevated temperature using ANN. *Measurement* **2019**, *147*, 106870. [CrossRef]
51. Liu, Q.-f.; Iqbal, M.F.; Yang, J.; Lu, X.-y.; Zhang, P.; Rauf, M. Prediction of chloride diffusivity in concrete using artificial neural network: Modelling and performance evaluation. *Constr. Build. Mater.* **2021**, *268*, 121082. [CrossRef]
52. Ramadan Suleiman, A.; Nehdi, M.L. Modeling Self-Healing of Concrete Using Hybrid Genetic Algorithm–Artificial Neural Network. *Materials* **2017**, *10*, 135. [CrossRef]
53. Šipoš, T.K.; Miličević, I.; Siddique, R. Model for mix design of brick aggregate concrete based on neural network modelling. *Constr. Build. Mater.* **2017**, *148*, 757–769. [CrossRef]
54. Getahun, M.A.; Shitote, S.M.; Abiero Gariy, Z.C. Artificial neural network based modelling approach for strength prediction of concrete incorporating agricultural and construction wastes. *Constr. Build. Mater.* **2018**, *190*, 517–525. [CrossRef]
55. Tran, V.-L.; Thai, D.-K.; Nguyen, D.-D. Practical artificial neural network tool for predicting the axial compression capacity of circular concrete-filled steel tube columns with ultra-high-strength concrete. *Thin-Walled Struct.* **2020**, *151*, 106720. [CrossRef]
56. Roshani, M.M.; Kargar, S.H.; Farhangi, V.; Karakouzian, M. Predicting the effect of fly ash on concrete's mechanical properties by ann. *Sustainability* **2021**, *13*, 1469. [CrossRef]
57. Yüzer, N.; Akbaş, B.; Kızılkanat, A.B. Predicting the compressive strength of concrete exposed to high temperatures with a neural network model. In Proceedings of the TÇMB, 3rd International Symposium Sustainability in Cement and Concrete, İstanbul, Turkey, 21–23 May 2007.
58. Goh, A.T. Back-propagation neural networks for modeling complex systems. *Artif. Intell. Eng.* **1995**, *9*, 143–151. [CrossRef]
59. Benardos, P.G.; Vosniakos, G.-C. Optimizing feedforward artificial neural network architecture. *Eng. Appl. Artif. Intell.* **2007**, *20*, 365–382. [CrossRef]
60. Mousavi, A.; Hajiloo, H.; Green, M.F. Bond Performance of GFRP Reinforcing Bars under Uniform or Gradient Temperature Distributions. *J. Compos. Constr.* **2021**, *25*, 04021056. [CrossRef]
61. Yusuf, M.; Sarhat, S.; Hajiloo, H.; Green, M.F. Bond strength between steel reinforcement and RCA concrete during and after exposure to elevated temperatures. *Constr. Build. Mater.* **2022**, *345*, 128362. [CrossRef]
62. *ACI 216.1-14*; Code Requirements for Determing Fire Resistance of Concrete and Masonry Construction Assemblies. American Concrete Institute: Farmington Hills, MI, USA, 2014.
63. *EN 1992-1-2 (2004)*; Design of Concrete Structures-Part 1–2: General Rules-Structural Fire Design. European Committee for Standardization: Brussels, Belgium, 2004; Volume 1, p. 1.
64. Ma, Q.; Guo, R.; Zhao, Z.; Lin, Z.; He, K. Mechanical properties of concrete at high temperature—A review. *Constr. Build. Mater.* **2015**, *93*, 371–383. [CrossRef]

65. Fu, Y.F.; Wong, Y.L.; Poon, C.S.; Tang, C.A. Stress-strain behaviour of high-strength concrete at elevated temperatures. *Mag. Concr. Res.* **2005**, *57*, 535–544. [CrossRef]
66. Pliya, P.; Hajiloo, H.; Romagnosi, S.; Cree, D.; Sarhat, S.; Green, M. The compressive behaviour of natural and recycled aggregate concrete during and after exposure to elevated temperatures. *J. Build. Eng.* **2021**, *38*, 102214. [CrossRef]
67. Felicetti, R.; Gambarova, P.G. Effects of high temperature on the residual compressive strength of high-strength siliceous concretes. *ACI Mater. J.* **1998**, *95*, 395–406.
68. Chan, S.Y.N.; Peng, G.-f.; Chan, J.K.W. Comparison between high strength concrete and normal strength concrete subjected to high temperature. *Mater. Struct.* **1996**, *29*, 616. [CrossRef]
69. Aydın, S.; Baradan, B. Effect of pumice and fly ash incorporation on high temperature resistance of cement based mortars. *Cem. Concr. Res.* **2007**, *37*, 988–995. [CrossRef]
70. Karahan, O. Transport properties of high volume fly ash or slag concrete exposed to high temperature. *Constr. Build. Mater.* **2017**, *152*, 898–906. [CrossRef]
71. Suzuki, M.; Mizukami, K. Bond strength between cement paste and aggregate. In Proceedings of the Review 30th General Meeting, Japan, Tokyo, June 1976; pp. 211–213.
72. Lyubimova, T.Y.; Pinus, E. Crystallization structure in the contact zone between aggregate and cement in concrete. *Colloid J. USSR* **1962**, *24*, 491–498.
73. Patten, B.J.F. The effects of adhesive bond between coarse aggregate and mortar on the physical properties of concrete. *Inst. Eng. (Aust.) Civ. Eng. Trans.* **1973**, *CE15*, 58–62.
74. Lee, W.; Van Deventer, J. Chemical interactions between siliceous aggregates and low-Ca alkali-activated cements. *Cem. Concr. Res.* **2007**, *37*, 844–855. [CrossRef]
75. Khedmati, M.; Kim, Y.-R. Multiscale characterization to examine the effects of aggregate properties on aggregate-paste interphase in cement concrete mixtures. *J. Mater. Civ. Eng.* **2020**, *32*, 04020059. [CrossRef]
76. Perry, C.; Gillott, J.E. The influence of silica fume on the strength of the cement-aggregate bond. *Spec. Publ.* **1995**, *156*, 191–212.
77. Chatterji, S.; Jeffery, J.W. The nature of the bond between different types of aggregates and Portland cement. *Indian Concr. J.* **1971**, *45*, 346–349.
78. Struble, L.; Skalny, J.; Mindess, S. A review of the cement-aggregate bond. *Cem. Concr. Res.* **1980**, *10*, 277–286. [CrossRef]
79. Ahmad, S.; Sallam, Y.S.; Al-Hawas, M.A. Effects of key factors on compressive and tensile strengths of concrete exposed to elevated temperatures. *Arab. J. Sci. Eng.* **2014**, *39*, 4507–4513. [CrossRef]
80. Sarhat, S.R.; Sherwood, E.G. Residual mechanical response of recycled aggregate concrete after exposure to elevated temperatures. *J. Mater. Civ. Eng.* **2013**, *25*, 1721–1730. [CrossRef]
81. Xu, Y.; Wong, Y.; Poon, C.S.; Anson, M. Impact of high temperature on PFA concrete. *Cem. Concr. Res.* **2001**, *31*, 1065–1073. [CrossRef]
82. Tai, Y.-S.; Pan, H.-H.; Kung, Y.-N. Mechanical properties of steel fiber reinforced reactive powder concrete following exposure to high temperature reaching 800 °C. *Nucl. Eng. Des.* **2011**, *241*, 2416–2424. [CrossRef]
83. Castillo, C. *Effect of Transient High Temperature on High-Strength Concrete*; Rice University: Houston, TX, USA, 1987.
84. Piasta, J.; Sawicz, Z.; Rudzinski, L. Changes in the structure of hardened cement paste due to high temperature. *Matériaux Constr.* **1984**, *17*, 291–296. [CrossRef]
85. Vedalakshmi, R.; Raj, A.S.; Srinivasan, S.; Babu, K.G. Quantification of hydrated cement products of blended cements in low and medium strength concrete using TG and DTA technique. *Thermochim. Acta* **2003**, *407*, 49–60. [CrossRef]
86. Ukrainczyk, N.; Ukrainczyk, M.; Šipušić, J.; Matusinović, T. XRD and TGA investigation of hardened cement paste degradation. In Proceedings of the Conference on Materials, Processes, Friction and Wear, Vela Luka, Croatia, 22–24 June 2006; pp. 22–24.
87. Jennings, H.M. Refinements to colloid model of C-S-H in cement: CM-II. *Cem. Concr. Res.* **2008**, *38*, 275–289. [CrossRef]
88. Ohno, I.; Harada, K.; Yoshitomi, C. Temperature variation of elastic constants of quartz across the α-β transition. *Phys. Chem. Miner.* **2006**, *33*, 1–9. [CrossRef]
89. Razafinjato, R.N.; Beaucour, A.-L.; Hebert, R.L.; Ledesert, B.; Bodet, R.; Noumowe, A. High temperature behaviour of a wide petrographic range of siliceous and calcareous aggregates for concretes. *Constr. Build. Mater.* **2016**, *123*, 261–273. [CrossRef]
90. Hager, I. Behaviour of cement concrete at high temperature. *Bull. Pol. Acad. Sci. Tech. Sci.* **2013**, *61*, 145–154. [CrossRef]
91. Ozguven, A.; Ozcelik, Y. Effects of high temperature on physico-mechanical properties of Turkish natural building stones. *Eng. Geol.* **2014**, *183*, 127–136. [CrossRef]
92. Sancak, E.; Sari, Y.D.; Simsek, O. Effects of elevated temperature on compressive strength and weight loss of the light-weight concrete with silica fume and superplasticizer. *Cem. Concr. Compos.* **2008**, *30*, 715–721. [CrossRef]
93. Terro, M.J.; Sawan, J.S. Compressive strength of concrete made with silica fume at elevated temperatures. *Kuwait J. Sci. Eng.* **1998**, *25*, 129–144.
94. Liu, J.-C.; Tan, K.H.; Yao, Y. A new perspective on nature of fire-induced spalling in concrete. *Constr. Build. Mater.* **2018**, *184*, 581–590. [CrossRef]

95. Gyu-Yong, K.; Young-Sun, K.; Tae-Gyu, L. Mechanical properties of high-strength concrete subjected to high temperature by stressed test. *Trans. Nonferrous Met. Soc. China* **2009**, *19*, s128–s133.
96. Roufael, G.; Beaucour, A.-L.; Eslami, J.; Hoxha, D.; Noumowé, A. Influence of lightweight aggregates on the physical and mechanical residual properties of concrete subjected to high temperatures. *Constr. Build. Mater.* **2021**, *268*, 121221. [CrossRef]